EXPERIMENTAL AND ANALYTICAL DETERMINATION OF FRICTION TORQUE OF A DOUBLE ROW ROLLER SLEWING BEARING

A THESIS SUBMITTED TO
THE GRADUATE SCHOOL OF NATURAL AND APPLIED SCIENCES
OF
MIDDLE EAST TECHNICAL UNIVERSITY

BY

AHMET DİNDAR

IN PARTIAL FULFILLMENT OF THE REQUIREMENTS
FOR
THE DEGREE OF MASTER OF SCIENCE
IN
MECHANICAL ENGINEERING

DECEMBER 2015

Approval of the thesis:

EXPERIMENTAL AND ANALYTICAL DETERMINATION OF FRICTION TORQUE OF A DOUBLE ROW ROLLER SLEWING BEARING

submitted by **AHMET DİNDAR** in partial fulfillment of the requirements for the degree of **Master of Science in Mechanical Engineering Department, Middle East Technical University** by,

Prof. Dr. Gülbin Dural Ünver
Dean, Graduate School of **Natural and Applied Sciences** _____

Prof. Dr. R. Tuna Balkan
Head of Department, **Mechanical Engineering** _____

Prof. Dr. Mehmet Çalışkan
Supervisor, **Mechanical Engineering Dept., METU** _____

Prof. Dr. Metin Akkök
Co-Supervisor, **Mechanical Engineering Dept., METU** _____

Examining Committee Members:

Assoc. Prof. Dr. Ender Ciğeroğlu
Mechanical Engineering Dept., METU _____

Prof. Dr. Mehmet Çalışkan
Mechanical Engineering Dept., METU _____

Prof. Dr. Metin Akkök
Mechanical Engineering Dept., METU _____

Asst. Prof. Dr. Gökhan O. Özgen
Mechanical Engineering Dept., METU _____

Asst. Prof. Dr. Bülent İrfanoğlu
Mechatronics Engineering Dept., Atılım University _____

Date: 04.12.2015

I hereby declare that all information in this document has been obtained and presented in accordance with academic rules and ethical conduct. I also declare that, as required by these rules and conduct, I have fully cited and referenced all material and results that are not original to this work.

Name, Last name : Ahmet DİNDAR

Signature :

ABSTRACT

EXPERIMENTAL AND ANALYTICAL DETERMINATION OF FRICTION TORQUE OF A DOUBLE ROW ROLLER SLEWING BEARING

Dindar, Ahmet
M.S, Department of Mechanical Engineering
Supervisor : Prof. Dr. Mehmet Çalışkan
Co-supervisor : Prof. Dr. Metin Akkök

December 2015, 81 pages

Friction at low speeds is accepted as the most dominant destabilizing factor in gun turrets, since precise aiming to the target is conducted at low speeds. So, the causes and mechanisms of friction in gun turrets should be investigated. The friction is mainly caused by the bearings in the rotation axes.

In this thesis, investigation on the friction torque of a double row roller slewing bearing which is operated in the azimuth axis of a gun turret is performed. For this purpose, a friction measurement test setup is designed and friction torque measurements are conducted. Tests are performed at various speeds and loading conditions. Friction sources are decoupled and examined separately in order to fully understand effect of each component on friction torque of the slewing bearing. Therefore, friction caused by rolling motion and friction caused by two different types of lip seals are investigated. In addition, friction identification analyses are performed. In the analysis, load distribution of the bearing is calculated by finite element analysis software and

rolling motion is simulated with a multibody dynamic analysis program. Consequently, analyses results are compared and verified with the test results.

Keywords: Friction, Slewing Bearing, Lip Seal, Friction Measurement Test Setup, Experimental Validation

ÖZ

ÇİFT SIRA SİLİNDİRİK MASURALI DÖNER TABLA RULMANI SÜRTÜNME TORKUNUN DENEYSEL VE ANALİTİK OLARAK BELİRLENMESİ

Dindar, Ahmet
Yüksek Lisans, Makine Mühendisliği Bölümü
Tez Yöneticisi : Prof. Dr. Mehmet Çalışkan
Ortak Tez Yöneticisi : Prof. Dr. Metin Akkök

Aralık 2015, 81 sayfa

Silah kulelerinde hedefe hassas olarak yönelme düşük hızlarda gerçekleştirildiğinden düşük hızlardaki sürtünme torku stabilizasyonu bozan en önemli faktör olarak kabul edilmektedir. Bu sebeple, silah kulelerinde oluşan sürtünmenin sebebi ve mekanizmaları incelenmelidir. Sürtünmenin ana kaynağı dönme eksenlerinde bulunan rulmanlardır.

Bu tezde, bir silah kulesi yan ekseninde bulunan çift sıra silindirik masuralı döner tabla rulmanının sürtünme torku incelenmiştir. Bu amaçla, sürtünme torku ölçüm düzeneği tasarlanmış ve tork ölçüm testleri gerçekleştirilmiştir. Testler çeşitli hızlarda ve yükleme koşullarında tekrarlanmıştır. Döner tabla rulmanının bileşenlerinin sürtünmeye etkisinin tam olarak anlaşılabilmesi için sürtünmenin ana sebepleri ayrıştırılarak test edilmiştir. Böylece, dönme hareketinden kaynaklı sürtünme ile iki farklı döner mil keçesinden kaynaklı sürtünme ayrı ayrı değerlendirilmiştir. Bunun yanında, sürtünme torku analizleri gerçekleştirilmiştir. Döner tabla rulmanının yük dağılımı sonlu elemanlar analizi programı ile, masura yuvarlanma simulasyonu ise çok

cisim dinamik analiz programı ile gerçekleştirilmiştir. Sonuçta, analizler test sonuçları ile karşılaştırılarak doğrulanmıştır.

Anahtar Kelimeler: Sürtünme, Döner Tabla Rulmanı, Mil Keçesi, Sürtünme Ölçüm Test Düzeneği, Deneysel Doğrulama

To my family…

ACKNOWLEDGEMENTS

First of all, I would like to express my deepest gratitude to my supervisors Prof. Dr. Mehmet Çalışkan and Prof. Dr. Metin Akkök for their help, guidance, criticism and support throughout the study. It is a great honor to be able to work with them and to meet with their experience, knowledge and ideas.

I would like to thank to my unit leader Yankı Çelebi and co-workers Göksenin Çetin, Gökhan Öztürk, Hasan Can Özden and Deniz Savcıözen for their support, encouragements and help.

I am thankful to my company ASELSAN Inc. for the possibilities that made my work easier.

I would like to thank TUBITAK for supporting me with a scholarship during my studies.

Finally, I wish to express my sincere thanks to my parents, Şerife and Ali Dindar, my sister Aslı Sarıyerli and her husband Esat Sarıyerli for their supports, encouragements and patience.

TABLE OF CONTENTS

LIST OF FIGURES

FIGURES

LIST OF TABLES

TABLES

LIST OF SYMBOLS

b	half Hertzian width
$\bar{d}$	gear diameter
d	diameter
E’	effective modulus of elasticity
f	traction coefficient
F, F_f	friction force
F_a	axial force
F_c	centrifugal force
F_{ct}	contact force
F_g	gear force
F_n	normal force
F_r	radial force
F_t	tangential force
g_e	dimensionless elasticity parameter
g_v	dimensionless viscosity parameter
G	dimensionless material number
h’	dimensionless film parameter
h_{min}, h_c	minimum film thickness
I	moment of inertia
$I_{y'y'}$	inertia around y’y’ axis
K_1	spring stiffness for rectangular conjunctions
l	contact width
L_a	asperity load ratio (in percentage)
m	mass of the rotating cylinder
M_t	tilting moment
M_{total}	total friction torque

M_{rr}	rolling resistance torque
M_{sl}	sliding torque
M_{drag}	drag torque
M_{seal}	sealing torque
$\mathrm{n_{gearbox}}$	total reduction ratio of gearboxes
n_p	slewing gear – pinion gear ratio
N	normal load
p	average contact pressure
p_h	average hydrodynamic pressure
r	radius of the rotating cylinder
R	equivalent contact radius
T	total torque at load side
T_α	torque caused by inertial effect
T_f	friction torque
$\mathrm{T_{motor}}$	total torque at motor
T_{sensor}	total torque at torque sensor
T_u	torque caused by unbalance
u	rolling velocity
u_s	sliding velocity
U	dimensionless velocity number
ω	rotational speed
$\mathrm{\omega_{bearing}}$	bearing rotational speed
w_l	load per contact length
$\mathrm{\omega_{motor}}$	motor rotational speed
$\mathrm{\omega_{sensor}}$	sensor rotational speed
W	dimensionless load number
$\overline{W}$	weight of the load
a	pressure-viscosity coefficient
$\bar{\alpha}$	rotational acceleration
$\bar{\bar{\alpha}}$	pressure angle
δ_m	elastic deformation

η	viscosity under pressure
η_0	inlet viscosity
η_{gearbox}	combined efficiency of gearboxes
Λ	lubricant film parameter
μ_{bd}	traction coefficient under boundary lubrication
μ_{hd}	traction coefficient due to lubricant film
$\bar{\sigma}$	dimensionless surface roughness number
v	poisson's ratio
τ	shear stress
τ_{lim}	limiting shear stress

LIST OF ABBREVIATIONS

EHD	elastohydrodynamic
TEHD	thermoelastohydrodynamic
DC	direct current
3D	3-dimensional
EHL	elastohydrodynamic lubrication
FEA	finite element analysis

CHAPTER 1

INTRODUCTION

Gun turret system, also called stabilized gun platform, is an unmanned stabilized weapon mount which is used to position and fire the weapon to targets. In early designs of gun turrets, positioning and firing is made by soldiers. However, in today's designs, positioning and firing is automated. In order to aim to a target in 3D space, gun turret subsystems have two degrees of freedom in the elevation and azimuth axes. Positioning of the turret is done by actuators which gives motion to the turret in these axes.

Figure 1.1 A gun turret system (Photo Courtesy of ASELSAN Inc.)

Gun turrets can be mounted and used either on a stable platform or on a moving land or naval vehicle such as tank, ship etc. For the ones mounted on moving vehicles, disturbances coming from the vehicle make the stabilization more difficult. Since performance of a gun turret directly relates to its movement and stabilization capabilities, it is vital to perfect the stabilization of the turret.

In the following sections of this chapter, general information about slewing bearings and friction phenomena is presented.

1.1. Double Row Roller Slewing Bearing

Slewing bearings are large diameter, high load capacity anti-friction bearings. They are used widely in the industry such as aerospace and defense, heavy equipment, industrial machinery, renewable energy etc. as slewing bearings can withstand high loads in axial, radial and tilting axes. According to the technical requirements, slewing bearings may be produced up to 8- meter diameters as monobloc and even higher diameters as segmental bearings [1].

There are different types of slewing bearings in market. According to bearing element type, classification is made as ball bearings, roller bearings and combination of ball and roller bearings (Figure 1.2).

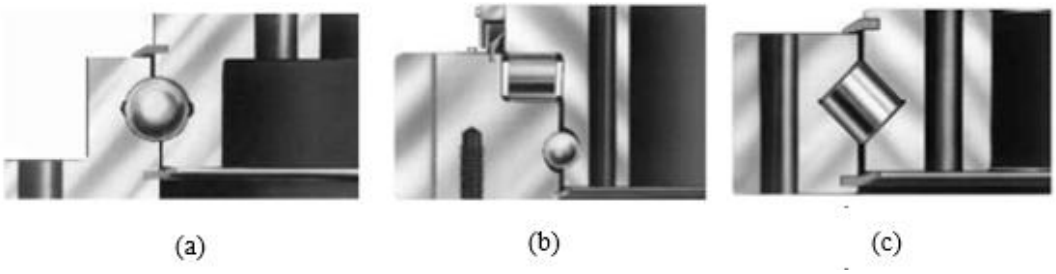

Figure 1.2 Section views of slewing bearings according to roller element types: (a) Ball Bearing, (b) Ball and Roller Bearing, (c) Roller Bearing [1]

Slewing bearings may have multiple rows of bearing elements such as double-row and triple-row slewing bearings (Figure 1.3).

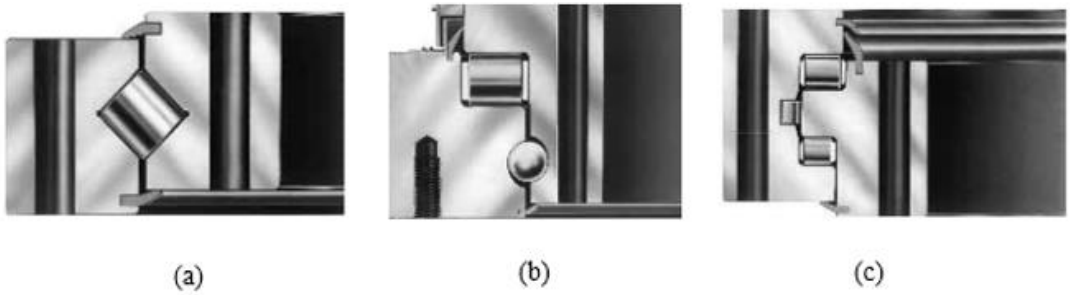

Figure 1.3 Section views of slewing bearings according to number of rows: (a) Single row Roller bearing, (b) Double Row Ball and Roller Bearing, (c) Triple Row Roller Bearing [1]

Another classification of slewing bearings is made according to their actuation input type such as slewing bearing with internal gear, slewing bearing with external gear and slewing bearing without gear.

The type of the slewing bearing being investigated in this thesis is a three wire-race double row roller bearing (Figure 1.4). Wire-race bearing is a special type of slewing bearing, that is, it is made lighter by using aluminum inner and outer rings instead of steel. However, for the load to be supported, the race is composed of steel wires.

Wire-race slewing bearing is mainly composed of six types of parts: inner ring, outer ring, rolling elements, raceways, seals and cages. Relative motion occurs between inner and outer rings while rolling elements roll between wire races. Cage keeps rolling elements in equidistant positions, hence prevents any collision between rolling elements. Seal is used for not only to keep contaminants out but also to keep lubricants in. Usage of seals increases maintenance time period and prolongs the life of bearing by protecting bearing elements from dirt, dust, etc. In the slewing bearing, two different types of lip seals are used. One of the lip seals, located on the lower side, is tightened by a garter spring in order to increase the efficiency of sealing. This is mainly because of the fact that lower seal is exposed to harsh environments more than the upper seal.

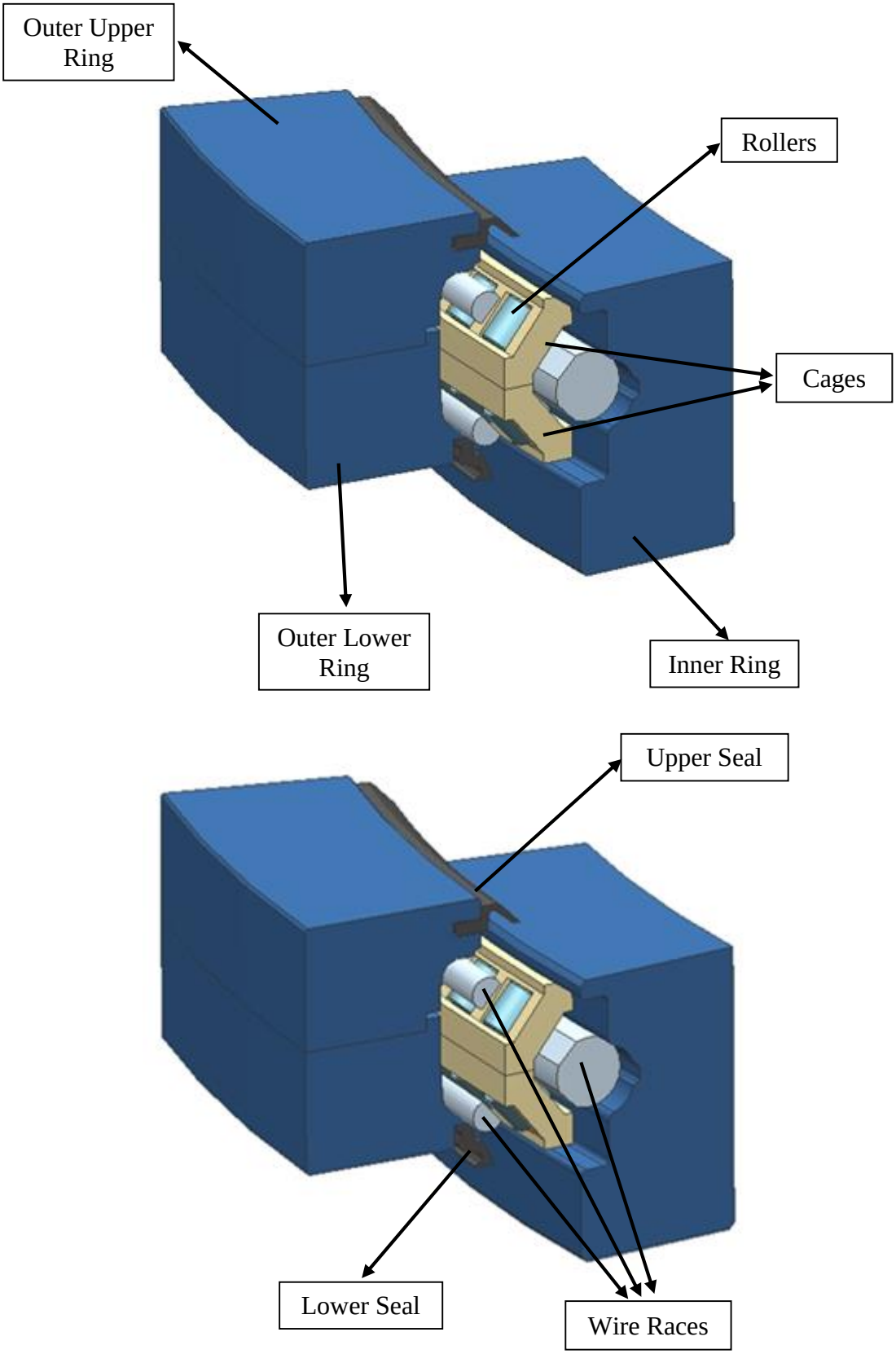

Figure 1.4 Three wire-race double row roller bearing

1.2. Friction Sources in Bearings

Friction is defined as the resistance encountered when one body moves tangentially over another with which it is in contact [2]. Friction force opposes the work generating force and turns this work into heat. Because of that, friction should be avoided or decreased in system design, unless the friction is to be used as a tool for force transmission such as in automobile tires on a road way, vehicle brakes and clutches etc. [2].

Friction occurs in all of the contacts of a body with its environment. So, frictional behavior of a slewing bearing can only be understood, if all of the possible sources of friction are investigated. Friction sources of a bearing can be examined in three major topics which can be listed as

- Torque due to applied load
- Viscous friction torque
- Seal friction torque

1.2.1. Torque Due To Applied Load

Elastic hysteresis is one of the sources of the friction. When rolling elements rolls over the races, front side of the roller that is the leading edge is compressed while trailing edge relieves. The deflection that occurs as load is increasing in a specified stress level is smaller than the deflection that occurs as load is decreasing. This phenomena is called as elastic hysteresis [3].

Secondly, **deformation of the rollers and the raceways** is another source of friction in bearings. When the load is applied, stress occurs in the contact area of both the roller and the raceway. The deflection, caused by the stress, creates an offset between the normal load axis and roller rotation axis resulting in a resisting moment. Similarly, while the rolling motion continues, raceway material is squeezed and raceway forms bulge in the leading edge of the contact (Figure 1.5).

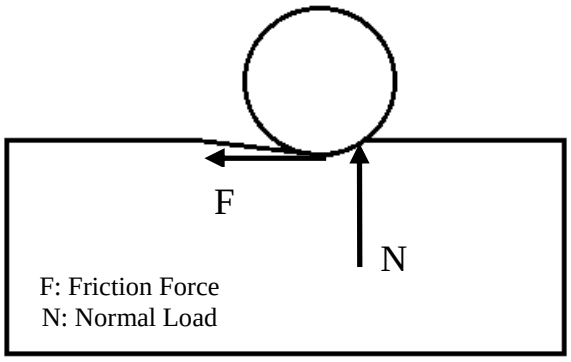

Figure 1.5 Deformation of raceway

Thirdly, **sliding** of bearing elements (other than seals) with respect to each other causes friction. Sliding friction is classified as [3]

- Sliding friction in rolling element – raceway contact
- Sliding friction between the cage and bearing rings
- Sliding friction between rolling elements and cage pockets
- Sliding between roller ends and ring flanges

1.2.2. Viscous Friction Torque

In general, bearings are lubricated in order to decrease friction, wear and heat generation. For normal operating conditions, lubricant separates contact surfaces by generating self-pressurized thin film layer between surfaces [4]. Although lubricant decreases rolling friction, it causes viscous friction since the lubricant resists the motion. In bearing lubrication, different lubrication methods can be used such as oil bath, circulating oil system, oil jet, greasing etc.

In the wire-race slewing bearing, grease lubrication is used. Grease lubrication is preferred because of its cheapness, long maintenance time, sealing easiness and favorable friction torque and temperature rise compared to oil lubrication. However,

grease is not suitable for high rotational speed bearings and does not flush out wear particles as in oil lubrication [4].

1.2.3. Seal Friction Torque

Seals are used in order to prevent leakage of lubricants from the bearing and to keep pollutants out of the bearing by creating an interface between rotary and stationary parts. Although, usage of seals increase maintenance time and provide good operation of the bearing, increase in friction is unavoidable.

The most commonly used seal type is rotary lip seals [4]. Schematic of a lip seal is displayed in Figure 1.6. Rotary lip seals consist of steel frame, elastomeric ring and garter spring. Steel frame is attached to the stationary part of the bearing and elastomeric ring. Tip point of the elastomeric ring touches the rotary part and separates oil and air sides. In some type of lip seals, garter spring is used. Main aim of a garter spring is to maximize sealing performance by increasing normal load of elastomeric ring on the shaft. Garter spring is used in applications with harsh environment conditions.

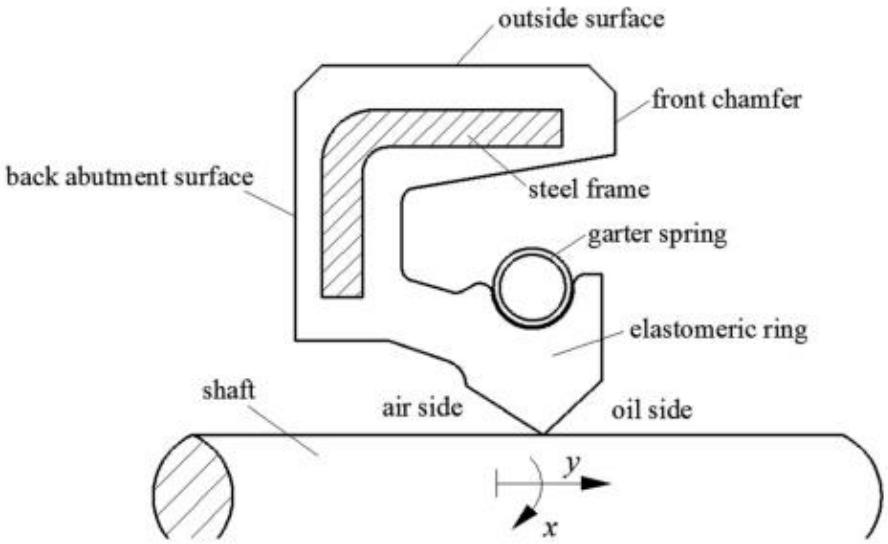

Figure 1.6 Schematic of a Lip [5]

In the wire-race slewing bearing, two lip seals are used between the inner and outer rings. One lip seal without a garter spring is used in the inner part of the slewing bearing, which is going to be called as upper seal in this thesis. Second lip seal is located in the outer part of the bearing, which is going to be called as lower seal in this thesis. Since lower seal is exposed to severe environmental conditions in the outer part of the bearing, a garter spring is used in the lower seal.

1.3. Goal of the Study

According to studies, friction at low speeds is accepted as the most dominant destabilizing factor in gun turrets since the final precise aiming to the target is conducted at low speeds [6]. So, the causes and mechanisms for friction in gun turrets should be investigated. In a rotation axis of a turret, friction force is mainly caused by the bearing.

In this thesis, investigation on the friction torque of a slewing bearing which is operated in the azimuth axis of a gun turret is performed. Friction torque measurement results are investigated and compared with analysis results. Friction sources are decoupled and examined separately in order to fully understand effect of each component on friction torque of the slewing bearing. By this way, this thesis provides the designer a good knowledge to improve friction characteristics of the slewing bearing. Moreover, a valid friction torque estimation of the slewing bearing under different load conditions can be simulated without the need of tests at the design stage.

In literature, several research studies have been carried to investigate bearing torques including different ball and roller bearing types. However, to the best of author's knowledge, no report has been found so far investigating the frictional behavior of slewing bearings. The primary goal of this study was to determine sources of friction and simulate them by both analytical and numerical methods.

1.4. Scope of the Study

The remainder of the thesis may be outlined as below:

In Chapter 2, previous works by other authors are studied. Studies about slewing bearings including load capacity analysis and fatigue lifetime analysis are investigated. In addition, studies about friction torque analysis and measurement techniques of bearings are stated. Finally, friction characteristics of lip seals are reviewed.

In Chapter 3, friction identification tests are presented. Design details of friction measurement test setup, which is used to conduct the tests, are given in this chapter. Test procedure and friction torque calculation method is presented. In addition, test results for different speed and loading conditions are provided and discussed.

In Chapter 4, friction torque analysis of the slewing bearing is performed. A finite element program is used to determine load distribution of the slewing bearing and to obtain roller raceway contact forces in combined loading conditions. Then, a multibody dynamic model is generated in order to simulate rolling friction of the bearing. Moreover, a simple numerical analysis is made for seals by using test results. In this chapter, comparison of the test results and the analyses is presented by discussing possible reasons for differences.

In Chapter 5, summary of the thesis is given with main conclusions of the tests and analyses. Moreover, recommendations for future research are supplied.

CHAPTER 2

LITERATURE SURVEY

In this chapter, literature survey on the studies about load carrying capacity of slewing bearings and friction measurements and analyses of bearings are presented.

2.1. Static and Dynamic Analysis of Slewing Bearings

Previous studies about slewing bearings have primarily concentrated on static and dynamic load capacity calculation. In addition, life prediction calculations of slewing bearings are performed.

Amasorrain et al [7] presented a calculation procedure for determining load distribution in the rolling elements of a four point contact slewing bearing. The given procedure is an extension to four point contact of the general bearing theory. Glodez et al [8] presented a computational method for determination of static capacity of a four point contact slewing bearing. Then, fatigue lifetime of the slewing bearing is calculated in three different approaches and compared: ISO standardized calculation approach, a stress-life approach and a strain-life approach. Pandiyarajan et al [9] performed stress analysis of contacts in large diameter ball bearings with both analytical and numerical methods. In the study, comparisons between the results of analytical and numerical solutions are conducted.

Kania et al [10] carried out a study on a method to calculate catalogue capacity of a slewing bearing by FE models. In their work, they take into account the effect of flexural-torsional flexibility of bearing rings and flexibility and number of bearing

clamping bolts. In another study, Kania [11] studied the deformation of slewing bearings due to unequal loading. By replacing rolling elements with truss elements in finite element models, he calculated the deflection of a slewing bearing.

Aguirrebeitia et al [12] performed a study on the derivation of general static load-carrying capacity of three row roller slewing bearing under axial and tilting moment. They provided an acceptance curve in the load space which offers an approximate quick way for the design and selection of the slewing bearing.

Göncz et al [13] investigated load capacity of a three-row roller slewing bearing raceway. Numerical calculations of subsurface stress field and fatigue life prediction with two different types of rollers were presented: a plain cylindrical roller and a profiled roller. In another study, static capacity of a double row slewing ball bearing with predefined irregular geometry was studied by Göncz et al [14]. In the study, a new calculation approach based on a vector description of a bearing geometry was presented. The calculation approach enables one to examine the effect of multi-row geometry and predefined irregular geometry of the bearing. In a different study, Göncz et al [15] presented a calculation procedure for determination of dynamic load capacity of large three row roller slewing bearings. In the study, determination of internal contact force, determination of stress field in the contact area and determination of the bearing's fatigue life by using stress life approach are carried.

Effect of clearances on the load distribution of a double row four point contact slewing bearing was investigated by Wang et Al [16]. In their study, a computational model which includes clearance effect is presented for determining force distribution and static load carrying capacity of the bearing and the results were discussed.

2.2. Bearing Friction Measurements and Analysis

Previous studies have primarily concentrated on friction torque measurement and modelling of ball and journal bearings.

Allmaier et al [17] carried out a study on prediction of friction in journal bearings. In their study, elastohydrodynamic (EHD) calculations, by an extensive oil-model considering roughness of contacting surfaces and different types of lubricants, are performed. Results of friction measurement tests were presented in order to verify the

model. In another study, Allmaier et al [18] extended previous work by including hydrodynamic pressure dependent oil-model. Consequently, it was shown that hydrodynamic pressure dependent oil model gives more reliable results for mixed lubrication regime whereas it does not change the results for full film lubrication. In a more recent research by Allmaier et al [19], EHD oil model improved to thermoelastohydrodynamic (TEHD) oil model which takes into account the effects of local temperature in the bearing.

Ünlü et al [20] performed experimental investigations to determine friction coefficient in journal bearings in variable speeds and loads. In the study, dependence of friction torque to bearing load and speed in dry and lubricated conditions is presented.

Friction moment analysis of a ball bearing is performed by Shaona et al [21]. In the paper, sources of friction in a ball bearing are investigated separately. Friction torque caused by bearing cage is found to be high in oscillatory motion, so analyses are done with different cage thicknesses and different clearances.

Friction torque in grease lubricated thrust ball bearings was studied by Cousseau et al [22]. Friction torques of thrust ball bearings lubricated with six different greases are measured to show the effect of viscosity of the grease base oil, coefficient of friction in full film condition and interaction between grease thickener and base oil. Moreover, bearing friction torque model developed by SKF [23] is compared with measurement results. The friction torque model classifies and models sources of friction in four groups as rolling torque, sliding torque, drag torque and sealing torque.

$$M_{total} = M_{rr} + M_{sl} + M_{drag} + M_{seal} \text{ [23]}$$

Similarly, Fernandes et al [24] investigated effect of gear oils on the friction torque of cylindrical roller thrust bearing. Test results were compared to SKF bearing friction torque model.

Joshi et al [25] studied running torque of double-arched angular contact bearing by improving a model and supporting the model with tests. Model disregards centrifugal and gyroscopic effects, covering high load and low speed applications. Friction sources are decoupled in spin, roll and hysteresis components and friction torque values are compared with previous friction torque models. In addition, verification of

the model is done with friction tests reported to show a good resemblance between model and experiment data.

Aihara [26] carried out a study on the friction torque formula for tapered roller bearings under axial load. Considering effects of rolling friction generated between raceways and rollers, and sliding friction between roller ends and inner ring rib, he developed a formulation. In the study, effect of sliding friction between rollers and cage pockets and influence of drag due to viscosity of lubricant are ignored. The model generated presents good agreement with friction torque values obtained from test data.

In a different study, Zhou and Hoeprich [27] carried out analytical analysis of torque of tapered roller bearings. Zhou and Hoeprich extended Aihara's friction torque calculation by using a different approach to the rib friction calculation and by enhancing raceway roller friction calculation. In the analysis, roughness effect of rib roller contact surfaces, influence of thermal EHL and lubricant parameter effects are considered. The analytical model is verified by the test data.

Qian [28] carried out a study on dynamic simulation of a cylindrical roller bearing. In the study, he used multi-body-dynamic simulation software to model the bearing completely considering roller pocket contact stiffness, cage geometry and elasticity of cage. Moreover, validation of analysis is done with tests.

2.3. Seal Friction Estimations and Analysis

Generally, seal is the most important factor of the friction torque in bearings. So, seal design and usage are very crucial in order to reduce friction torque of a bearing. In this section, previous studies performed on the relationship of seal design and friction torque of bearings are presented.

Marek [29] investigated main factors of rubber lip seals that affect frictional loss of sealing. He presented friction test results of seals with respect to changes in macro geometry, changes in micro geometry, lip and shaft material types, shaft geometry parameters and oil properties.

Plath et al [30] studied friction torque of a rotary shaft lip type seal. In the study, finite element analysis (FEA) of a lip seal is performed. In the analysis, lip seal is modeled

with Mooney Rivlin with two parameters and friction coefficient is taken as constant. In addition, friction measurement tests of the seal in different speed and temperature values are conducted by aerostatic, frictionless air bearing. In the end, comparison between test results and finite element simulation is done.

Similarly, Silvestri et al [31] presented friction torque analysis of a rotary lip seal by FEA and tests. Two different tests are performed in order to observe the overall friction and local behavior of seal portion. FEA results, numerical models available in literature and the test results are in good agreement.

In a different study, a wide-ranging model considering wear, friction and contact temperature of a radial shaft seal is developed by Frölich et al [32]. In the study, temperature change in seal lip due to contact pressure, wear and friction is modeled. Since material properties of elastomeric lip seals highly depend on temperature, modeling of temperature change in contact zone enables the designer to choose the right material for a specific application. Besides, by using empirical approaches friction and wear are simulated.

Lee at al [33] studied contact width and pressure distributions of lip seals. Results of FEA of rubber seal and experimental measurements are compared. It is concluded that both the numerical solutions and experiments can be used as design evaluation tools for lip seals.

Study of kinetic friction characterization of a tubular rubber seal is carried out by Ke et al [34]. In analysis part, theoretical model of kinetic friction with stick slip behavior is developed for the seal. A test rig is designed to measure normal force and friction force acting on the seal and sliding velocity of the seal. By using obtained data, effects of sliding velocities and normal loads on friction force are investigated.

CHAPTER 3

FRICTION IDENTIFICATION TESTS

3.1. Friction Measurement Test Setup

In order to measure the running torque of the slewing ring, a test setup is developed. The test setup consists of a DC servo motor, two gearboxes, a coupling, a torque sensor, a bearing unit and a pinion gear. The motion is transferred to the slewing bearing with the pinion gear supported with a bearing and coupled with the torque sensor. The torque sensor is supported with a leaf spring in order to prevent the rotation of its case. Motion is transferred from servo motor to the torque sensor by means of a coupling. The coupling couples the motion by allowing some angular and radial displacements between the torque sensor and servo motor, caused by manufacturing tolerances.

In order to determine motor and torque sensor capacities, the range of torques that will be applied to the setup during test is calculated. For a rotary system, three main factors resist motion: the friction torque, the torque caused by unbalance and the torque due to inertial effects.

- **Friction torque (T_f):** Friction torque occurs because of contacting surfaces. For capacity calculation considerations, the maximum friction torque of the slewing bearing is taken from the slewing bearing data sheet.

$$T_f = 23\ Nm$$

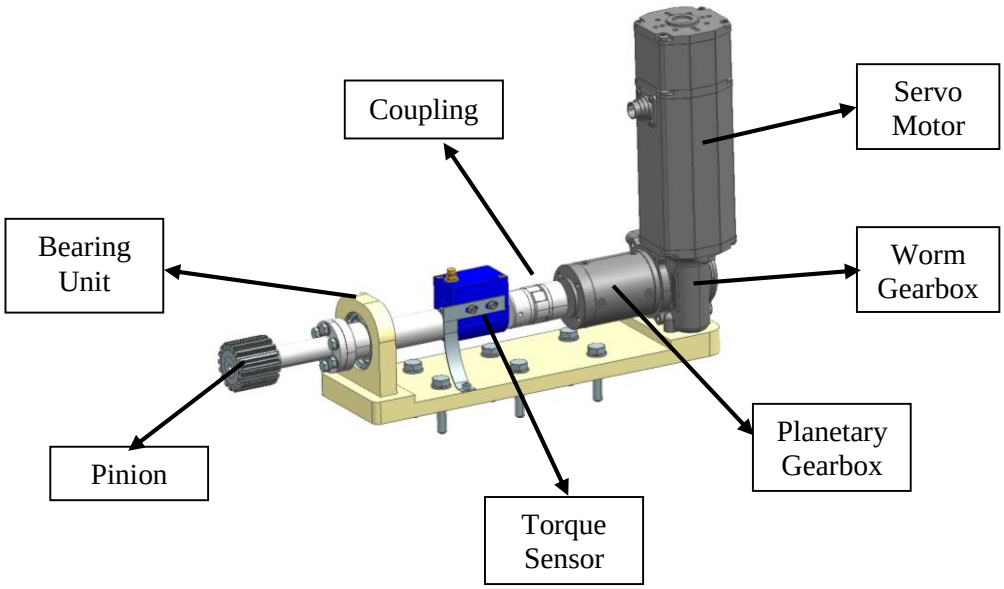

Figure 3.1 Friction Measurement Test Setup

- **Torque caused by unbalance (T_u):** Unbalance causes resisting torque if the center of mass of the system is at a different point than rotation axis and the center of mass of the system changes altitude while rotating. In the tests, center of mass does not change altitude since the rotation motion occurs in azimuth axis. So, the torque caused by unbalance is taken as 0.

$$T_u = 0$$

- **Torque due to inertial effect (T_α):** This torque occurs when there is rotational acceleration that is when the system speeds up or slows down.

$$T_\alpha = I.\bar{\alpha} = \frac{1}{2}.m.r^2.\bar{\alpha}$$

$\bar{\alpha}$: Rotational acceleration $(\frac{\text{rad}}{\text{s}^2})$

I: Inertia (kg.m^2)

m: Mass of the rotating cylinder (kg)

r: Radius of the rotating cylinder (kg. m^2)

$$T_\alpha = \frac{1}{2} x300x\ 0.4^2 x0.15 = \ 1.9\ Nm$$

In the above calculations, the inertia property is calculated as a cylinder rotating about its central axis. Angular acceleration α is taken as $0.15\ rad/s^2$ according to $4\ °/s^2$ whereas in friction identification tests, maximum slewing bearing rotation speed is determined as $4\ °/s$ and the slewing bearing is aimed to reach this speed in 1 s.

Then, the total torque affecting the torque sensor is calculated as,

$$T = \ T_u + T_\alpha + T_f = 26.6\ Nm$$

$$\mathrm{T_{sensor}} = \frac{\mathrm{T}}{\mathrm{n_p}} = \frac{26{,}6}{14{,}12} \cong 1.9\ \mathrm{N.m}$$

$$\omega_{\mathrm{sensor}} = \mathrm{n_p}.\,\omega_{\mathrm{bearing}} = 14.12\ \mathrm{x}\ 0.67 = 9.5\ \mathrm{rpm}$$

where

$\mathrm{n_p}$: Slewing gear − pinion gear ratio, $\quad \mathrm{n_p} = \frac{240}{17} = 14.12$

$$\omega_{bearing} = 4°/s \cong 0.67\ rpm$$

Moreover, the total torque affecting the motor is calculated as,

$$\mathrm{T_{motor}} = \frac{\mathrm{T_{sensor}}}{\mathrm{n_{gearbox}}.\,\eta_{\mathrm{gearbox}}} = \frac{1{,}9}{500\ \mathrm{x}\ 0.53} \cong 0.72\ \mathrm{N.cm}$$

$$\omega_{\mathrm{motor}} = \mathrm{n_{gearbox}}.\,\omega_{\mathrm{sensor}} = 500\ \mathrm{x}\ 9.5 = 4750\ \mathrm{rpm}$$

where

$\mathrm{n_{gearbox}}$: Total reduction ratio of the gearboxes, $\quad \mathrm{n_{gearbox}} = 500$

η_{gearbox}: Combined efficiency of the gearboxes, $\quad \eta_{\mathrm{gearbox}} = 0.53$

For 1.9 N.m torque value, the Lorenz Messtechnik DR-2112 torque sensor with 10 N.m capacity is selected. Selected servo motor is Dunker Motoren BG65x50 PI has continuous rated torque of 26 N.cm for 0.72 N.cm motor torque requirement. The torque of the selected motor is much higher than the calculated value. In order to be able to use the same test setup in possible future tests, the torque of the selected motor is much higher than needed.

Moreover, torque sensor and motor rotation speed is calculated as 9.5 rpm and 4750 rpm, respectively, and checked with torque sensor and motor limit speeds.

Figure 3.2 Servo Motor [35] and Torque Sensor [36]

Properties of the torque sensor and the servo motor are given in Table 3.1 and Table 3.2, respectively.

Table 3.1 Properties of DR-2112 Torque Sensor [36]

Lorenz Messtechnik – DR-2112	
Nominal Torque [N.m]	10
Accuracy Class Torque [% f.s.]	0.1
Mass [kg]	0.3
Limit Speed [1/min]	15000
Limit Thrust Load [N]	50

Table 3.2 Properties of BG65x50 PI Servo Motor [35]

Dunker Motor BG65x50 PI		
Rated voltage	VDC	24
Continuous rated speed	rpm	3100
Continuous rated torque	N.cm	26
Continuous current	A	5.6
Starting torque	N.cm	163
Peak current	A	27
Motor weight	kg	1.3

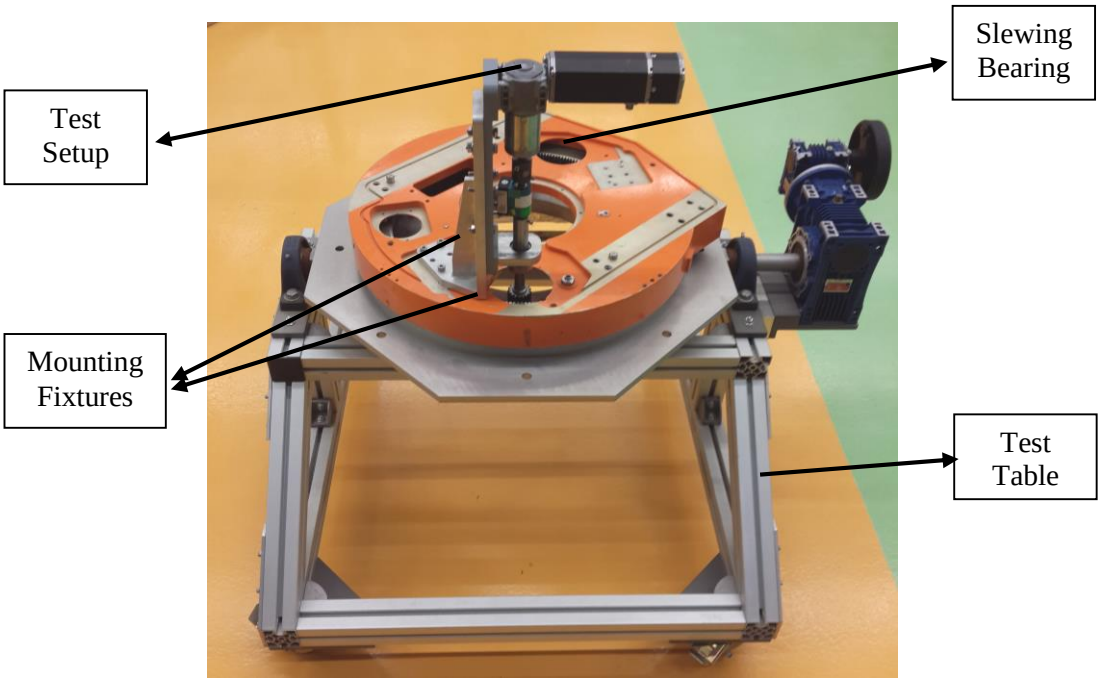

Figure 3.3 Friction Measurement Test Setup Assembly

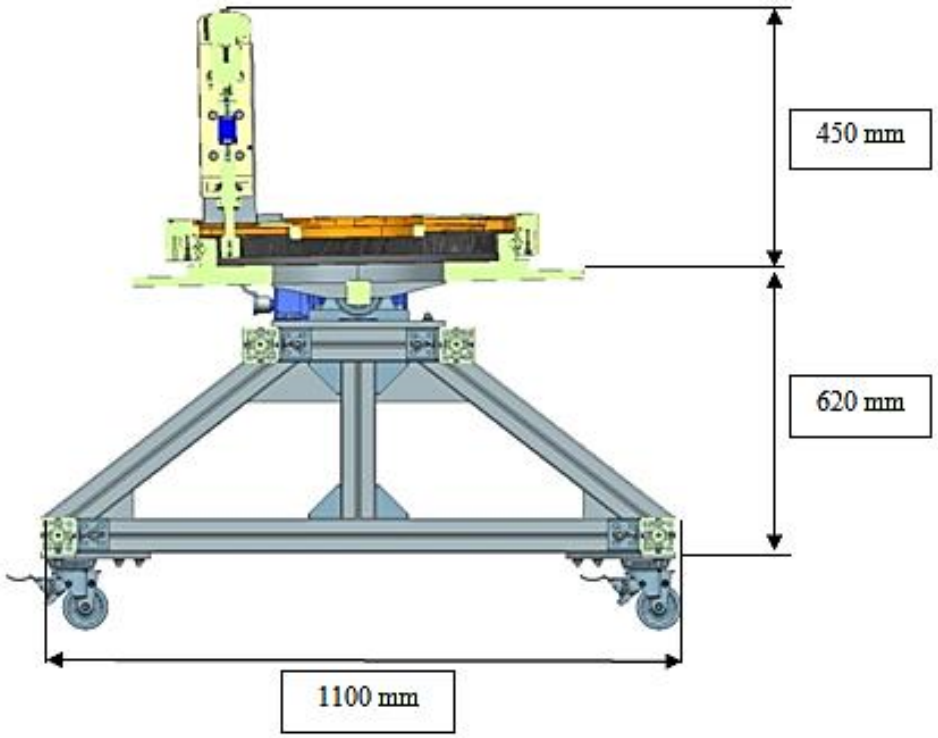

Figure 3.4 Section View of Friction Measurement Test Setup Assembly

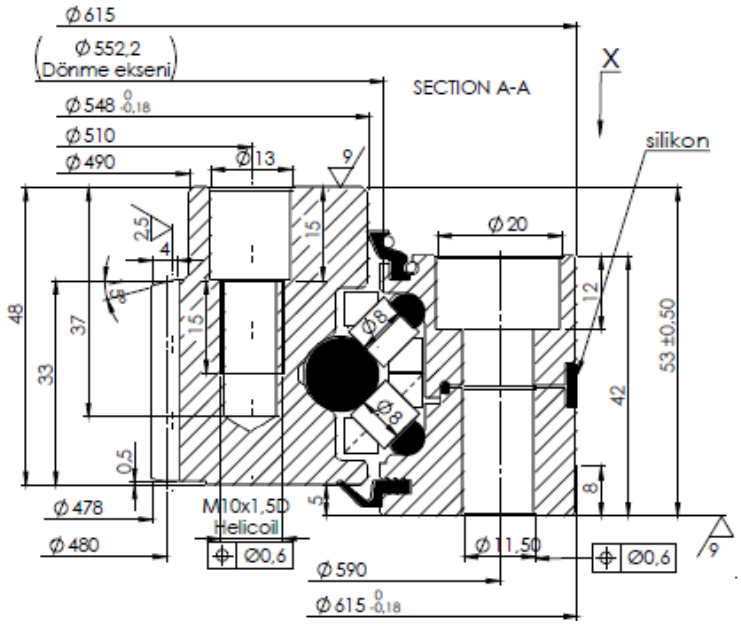

Figure 3.5 Section View of the Slewing Bearing (Dimensions are given in mm) (Photo Courtesy of ASELSAN Inc.)

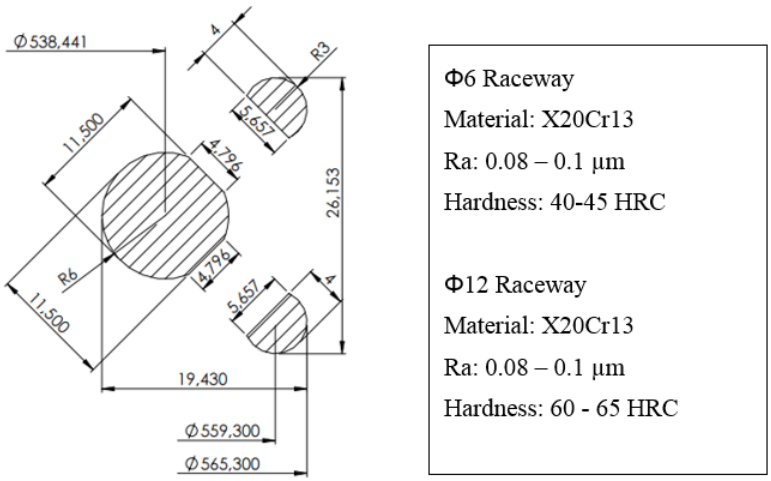

Figure 3.6 Technical Drawing of the Raceways (Photo Courtesy of TİBET Makina Inc.)

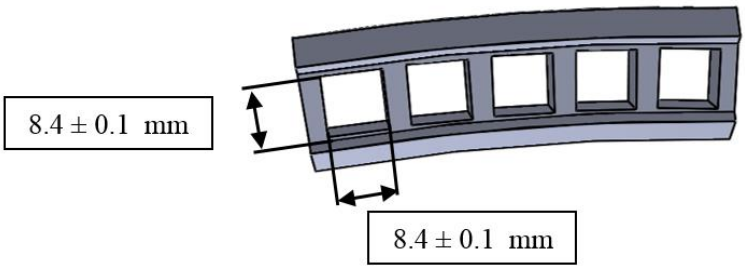

Figure 3.7 Drawing of the Cage

(Photo Courtesy of TİBET Makina Inc.)

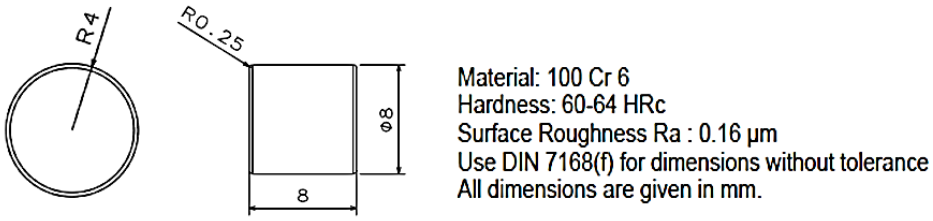

Figure 3.8 Techical Drawing of the Roller

(Photo Courtesy of TİBET Makina Inc.)

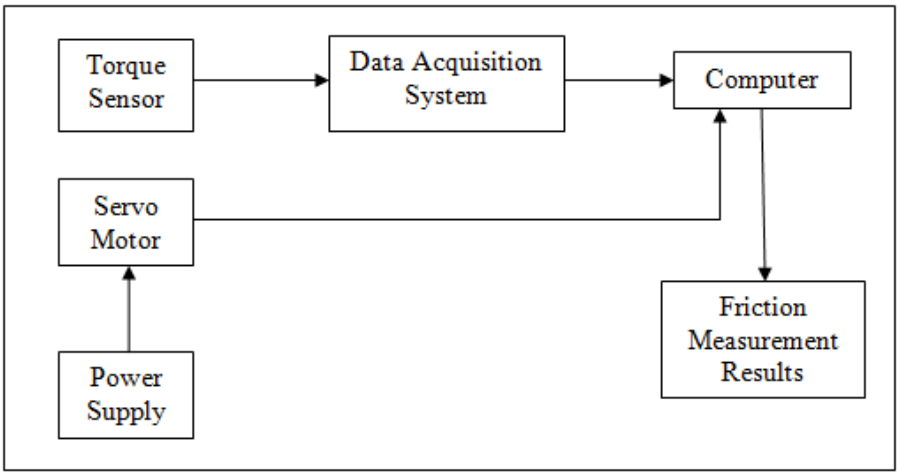

Figure 3.9 Connection Diagram of the Test Setup

Figure 3.3 shows the slewing bearing and torque measurement test setup assembly. Assembly consists of a test table, the slewing bearing, mounting fixtures and test setup. Firstly, mounting fixtures are fastened on outer ring of the slewing bearing. Next, mounting fixtures and slewing bearing subassembly are fixed on the test table by using mounting detail in the inner ring of the slewing bearing. Finally, the test setup is fixed to the mounting fixtures where pinion gear of the test setup mates with bearing gear. Mounting fixtures and test setup rotate around the rotation axis of the slewing bearing with respect to the test table by rotation of the pinion gear.

Figure 3.4 presents a section view of the test setup assembly. Dimensions of the test table are 1100 mm x 1100 mm x 620 mm. In Figure 3.5, section view of the slewing bearing and dimensions are given.

In Figures 3.6, 3.7 and 3.8, drawings of raceways, cage and roller are given, respectively.

Figure 3.9 presents friction measurement test setup connections. Servo motor is connected to power supply and computer. Guided user interface of the motor is used to change speed and position parameters. Moreover, speed and position feedback is obtained from the resolver of the motor. The torque sensor is connected to the computer via data acquisition system. The data acquisition system acquires voltage data from the torque sensor up to 100 kHz, while supplying power to the sensor. All the information is monitored and saved in the computer.

3.2. Test Procedure

Motion transfer diagram of the test assembly is given in Figure 3.10. In the tests slewing bearing, lower seal and upper seal are decoupled from the assembly in order to observe individual effects of each component.

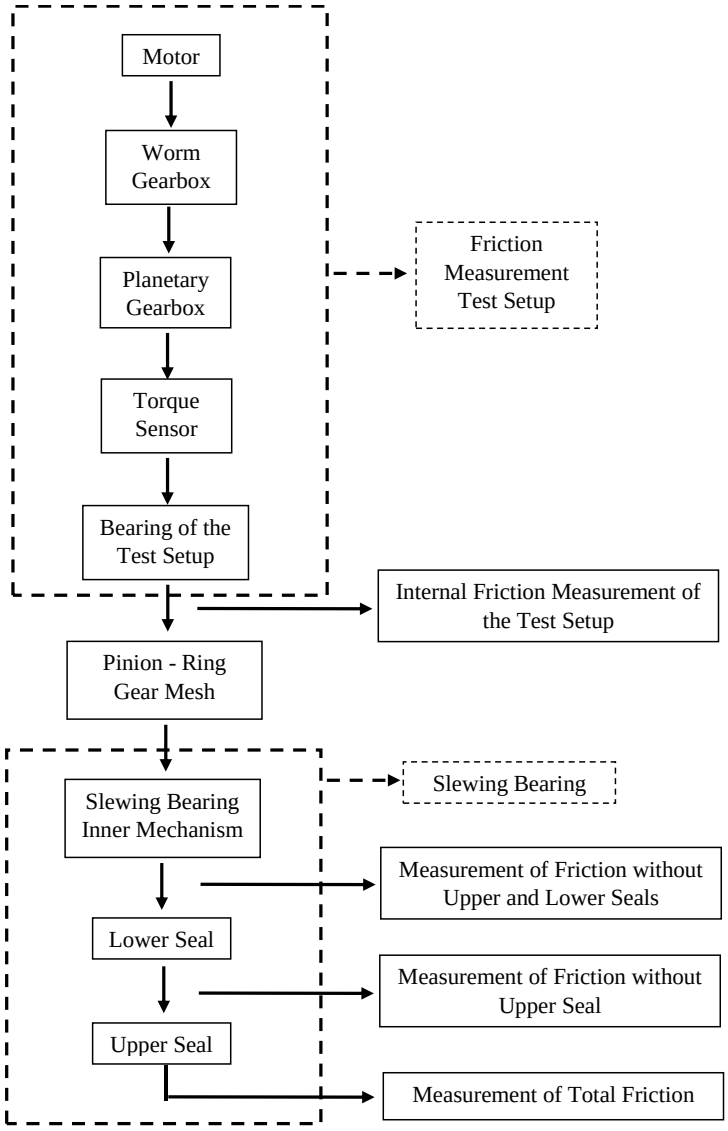

Figure 3.10 Friction Identification Tests Presented on Test Assembly Motion Transfer Diagram

3.2.1. Internal Friction Measurement of Test Setup

The friction measurement test setup is used to measure the friction torque of the slewing bearing. However, the test setup has an internal friction caused by the bearing

of the test setup. Since the friction of this bearing is out of consideration for this work, it should be eliminated. In order to measure the internal friction of the test setup, it should be mounted in the same orientation as the slewing bearing friction measurement tests to simulate the same effect of orientation of the test setup. As the frictional torque of the test setup is of interest only, pinion gear is not coupled with the slewing bearing gear. By this way, slewing bearing load is eliminated during the internal friction measurement of the test setup. However, influence of loading due to the gear mesh is ignored in these tests.

In order to see the effect of rotational speed on friction of the test setup, the same speed values are used in the tests as in "3.2.2. Slewing Bearing Friction Torque Measurement Tests". Motor rotational speeds are calculated by multiplying slewing bearing rotational speeds with the slewing gear / pinion gear ratio and the gearbox gear ratio which are 14.12 and 500, respectively.

3.2.2. Slewing Bearing Friction Torque Measurement Tests

Friction torque measurement of a slewing bearing is performed. Tests are done at different rotational speeds between 0.08 °/s and 3.82 °/s, for different axial loads between 200 N and 3200 N and for different tilting moment values between 0 Nm and 300 Nm. For each rotational speed and load combination, the bearing is driven with a constant speed in clockwise and counter-clockwise directions. In Figure 3.11, a test result is shown. In counterclockwise direction average friction torque is measured as 6.14 N.m, while in clockwise direction it is -6.34 N.m. The difference in the absolute torque values between clockwise and counterclockwise measurements arises from zero offset of the torque sensor. In order to eliminate this effect, foregoing friction torque calculations are made by averaging clockwise and counterclockwise torque values. That is, for this specific example (Axial Load = 1400 N and Velocity = 2.12 °/s) friction torque is calculated as 6.24 N.m.

In order to analyze individual effects of friction sources and to observe the effect of different loading conditions, a systematic approach is followed. Four groups of tests are applied in this procedure. These test configurations are given as:

i. **Measurement of Total Friction:** In this group of tests, running torque of the slewing bearing in its full configuration is measured for different loads starting from 200 N up to 3200 N axial load and for different bearing speeds from 0.08 °/s up to 3.82 °/s.

In order to eliminate the inherent internal friction torque of the test setup, the friction value found in part 3.2.1 is subtracted from the results of measurements of the total friction torque.

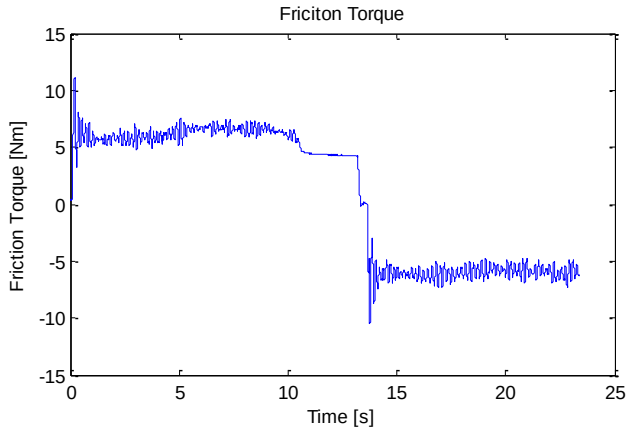

Figure 3.11 Sample Test Result (Load = 1400 N, Speed= 2.12 °/s)

ii. **Measurement of Friction without Upper Seal:** In this group of tests, all the tests given in Table 3.3 are performed by removing the upper seal of the bearing. In this way, the effect of upper seal in friction torque is eliminated. Then by comparing the results of "Measurement of Total Friction" and "Measurement of Friction without Upper Seal" tests, the friction torque due to the upper seal is obtained and examined.

iii. **Measurement of Friction without Upper and Lower Seals in Axial Loading:** In this group of tests, again all the tests given in Table 3.3 are performed by removing not only the upper seal but also the lower seal of the bearing. In this way, the contribution effect of upper and lower seals in friction torque is eliminated. The resultant friction torque values are due to rolling and sliding friction caused by contacts of bearing components and viscous friction caused by bearing lubrication. Moreover, results of these

tests are compared with the tests given in “Measurement of Friction without Upper Seal”. In the comparison, friction torque due to the lower seal is obtained and investigated.

Table 3.3 Axial Loading Test Steps

Test No.	Axial Load [N]	Rotational Speed [°/s]	Test No.	Axial Load [N]	Rotational Speed [°/s]	Test No.	Axial Load [N]	Rotational Speed [°/s]
1		0.08	27		0.08	53		0,08
2		0.17	28		0.17	54		0,17
3		0.25	29		0.25	55		0,25
4		0.42	30		0.42	56		0,42
5		0.64	31		0.64	57		0,64
6		0.85	32		0.85	58		0,85
7	200	1.27	33	1400	1.27	59	2600	1,27
8		1.7	34		1.7	60		1,7
9		2.12	35		2.12	61		2,12
10		2.55	36		2.55	62		2,55
11		2.97	37		2.97	63		2,97
12		3.4	38		3.4	64		3,4
13		3.82	39		3.82	65		3,82
14		0.08	40		0.08	66		0,08
15		0.17	41		0.17	67		0,17
16		0.25	42		0.25	68		0,25
17		0.42	43		0.42	69		0,42
18		0.64	44		0.64	70		0,64
19		0.85	45		0.85	71		0,85
20	800	1.27	46	2000	1.27	72	3200	1,27
21		1.7	47		1.7	73		1,7
22		2.12	48		2.12	74		2,12
23		2.55	49		2.55	75		2,55
24		2.97	50		2.97	76		2,97
25		3.4	51		3.4	77		3,4
26		3.82	52		3.82	78		3,82

iv. **Measurement of Friction without Upper and Lower Seals in Combined Loading:** This group of tests consists of friction torque measurement of the slewing bearing in combined loading conditions. In these tests, axial load is applied to the bearing with a tilting moment. Table 3.4 shows the loading conditions for each test step.

Table 3.4 Combined Loading Test Steps

Test No.	Moment [Nm]	Load [N]	Speed [°/s]	Test No.	Moment [Nm]	Load [N]	Speed [°/s]
1	0	800	0.08	31	180	2000	1.7
2			0.425	32			3.82
3			1.7	33		3200	0.08
4			3.82	34			0.425
5		2000	0.08	35			1.7
6			0.425	36			3.82
7			1.7	37	230	800	0.08
8			3.82	38			0.425
9		3200	0.08	39			1.7
10			0.425	40			3.82
11			1.7	41		2000	0.08
12			3.82	42			0.425
13	80	800	0.08	43			1.7
14			0.425	44			3.82
15			1.7	45		3200	0.08
16			3.82	46			0.425
17		2000	0.08	47			1.7
18			0.425	48			3.82
19			1.7	49	300	800	0.08
20			3.82	50			0.425
21		3200	0.08	51			1.7
22			0.425	52			3.82
23			1.7	53		2000	0.08
24			3.82	54			0.425
25	180	800	0.08	55			1.7
26			0.425	56			3.82
27			1.7	57		3200	0.08
28			3.82	58			0.425
29		2000	0.08	59			1.7
30			0.425	60			3.82

3.3.Test Results

In the scope of this work, five different groups of tests – 295 tests in total - are conducted. Firstly, in order to determine the internal friction of the test setup, constant speed torque values are measured for 13 different rotational speeds. In the second group of tests, the slewing bearing with its original configuration – with upper and lower seals intact- is tested for 13 different speeds and 6 different loading conditions. Third group of tests consist of measurement of the friction torque without upper seal in order to observe the effect of upper seal. In the fourth group, the lower seal is taken off, too. By doing this, friction torque of a slewing bearing free from seals is obtained. In addition, the effect of lower seal on the friction torque is derived by using third and fourth group of tests. In the last group of tests, friction torque measurement of the slewing bearing under combined loading is carried. These tests are performed without any seals in order to examine the effect of combined loading on the friction torque of the bearing. In Figures 3.12 and 3.13, the test setup with tilting moment and axial loading is presented, respectively.

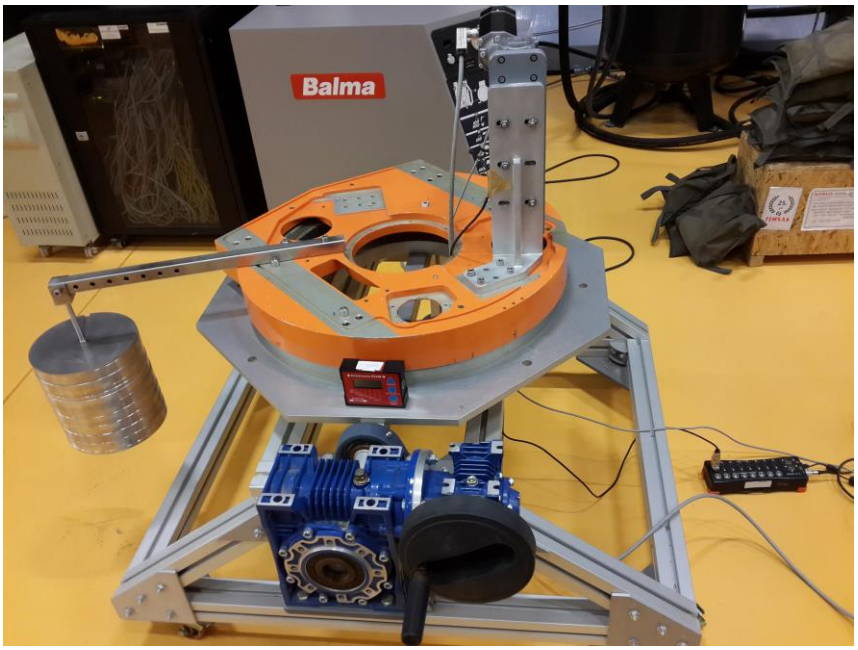

Figure 3.12 Combined Loading Tests

In this section, test results for the tests mentioned in section “3.2. Test Procedure” are presented.

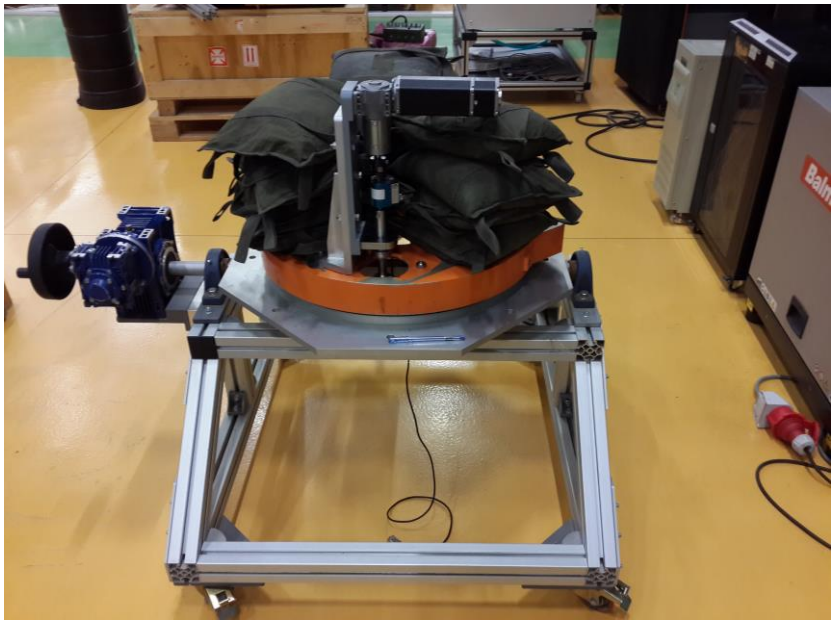

Figure 3.13 Axial Loading Tests

3.3.1. Internal Friction of Test Setup

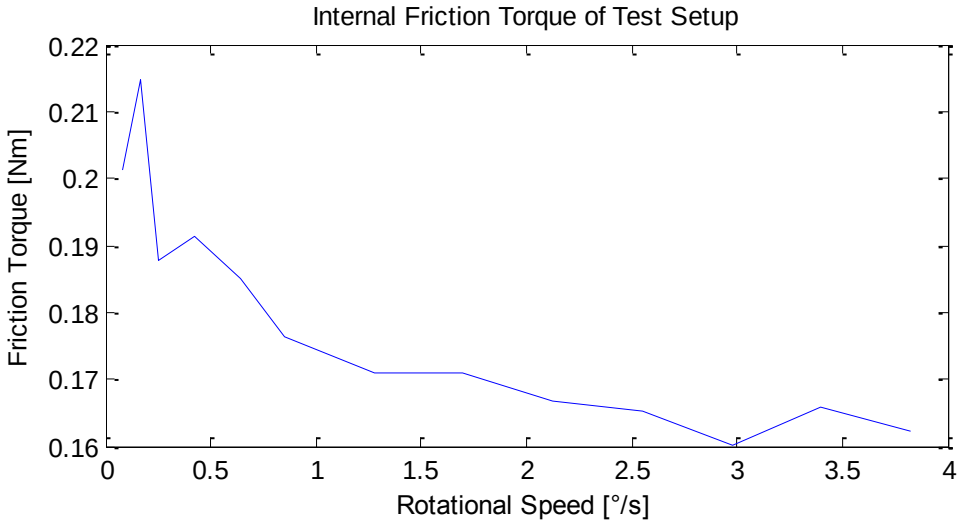

Figure 3.14 Internal Friction of Test Setup

Results of internal friction torque measurement are presented in Figure 3.14. Internal friction of the test setup changes between 0.16 N.m and 0.21 N.m. The general trend of the curve is such that, when the rotational speed increases, the friction torque

decreases, although there exist some discrepancies. Average internal friction torque is calculated as 0.18 N.m, which is, at some speeds, 14 % of the measured friction torque values. So, it is vital to subtract internal friction torque from the total bearing torque.

Differences with respect to rotational speed in internal friction of test setup are within maximum 3% of measured values. Although it seems small enough to determine an average internal friction and disregard the effect of rotational speed, the internal friction values are subtracted from the total friction figures according to corresponding speeds.

3.3.2. Friction Torque of the Slewing Bearing

As mentioned earlier, friction measurements are performed in different groups of tests with the aim of observing different frictional characteristics of bearing elements. When the test results are examined, the friction torque caused by lower seal, by the upper seal and by the bearing internal mechanism can be separated. In Figure 3.15, effects of these three factors on friction torque are presented with respect to rotational speed in axial loading. There are two important issues which must be drawn the attention. Firstly, 65.5% of the total friction is caused by sealing operation while the rest which amounts to 34.5% is caused by bearing internal friction. That is, sealing of the bearing increased the friction torque about twice as much.

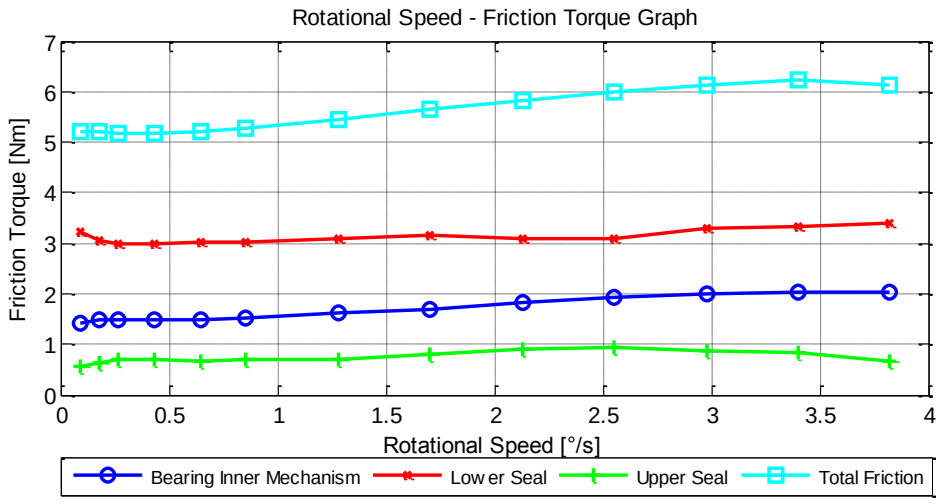

Figure 3.15 Friction torque as a function of rotational speed (Load = 1400 N)

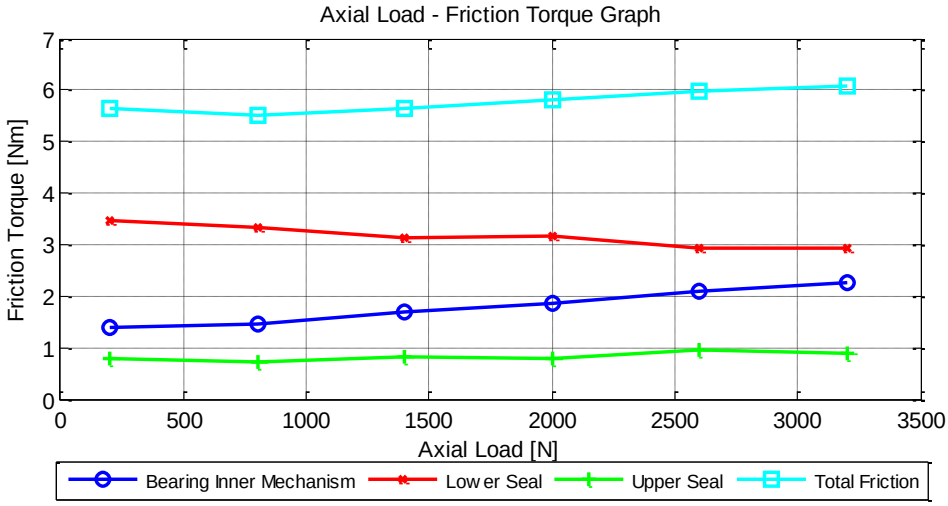

Figure 3.16 Friction torque as a function of axial load (Speed = 1.7 °/s)

Secondly, there is a major difference between the upper and lower seal friction torques. While the upper seal generates 10.7% of total bearing friction, the lower seal is responsible for 54.8% of total bearing friction, which is five times higher than that of the upper seal friction. This difference is caused by the sealing types. The upper seal is normal lip seal, since the upper part of the bearing is not exposed to harsh environmental effects. However, the lower seal is a lip seal with a garter spring in order to withstand harsh environments.

In Figure 3.16, the effects of the upper seal, lower seal and bearing internal mechanism on friction torque with respect to changes in axial load are shown. At low loads, the lower seal friction is about 60% of the total bearing friction while at high loads this value decreases down to 48%. Inversely, the bearing inner friction increases with load from 26% of total friction to 38%. The bearing inner friction is not affected by the load distribution at this level and it represents 14% of the total friction torque.

3.3.3. Bearing Inner Friction Torque in Axial Loading

Bearing inner friction torque arises from the resistance due to elastic hysteresis, deformation of the rollers and the raceways, sliding between bearing elements and viscous friction torque. In Figure 3.17, the bearing inner friction torque with respect to rotational speed is given. The bearing inner friction torque can be investigated in two

regions: rotational speeds below and above 0.3°/s. For the rotational speeds higher than 0.3°/s, the friction torque increases with increases in speed. This trend changes for the rotational speeds below 0.3 °/s. It looks that there is a dependence on load in this region. Up to 2000 N of axial load, the friction torque increases and then decreases slightly causing a local maximum at low speeds. However, for higher loads, the general trend of friction curves is decreasing, producing a local minimum.

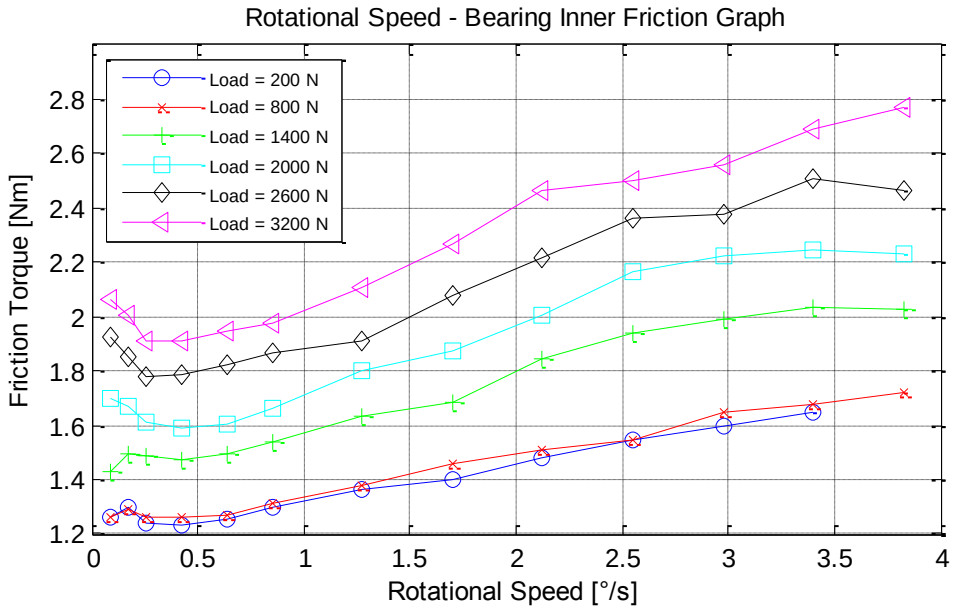

Figure 3.17 Bearing inner friction torque as a function of rotational speed at different axial loads

Dependence of bearing inner friction on load is presented in Figure 3.18. Up to 800 N load, friction does not change much. However, as the load increases more, friction increases almost linearly.

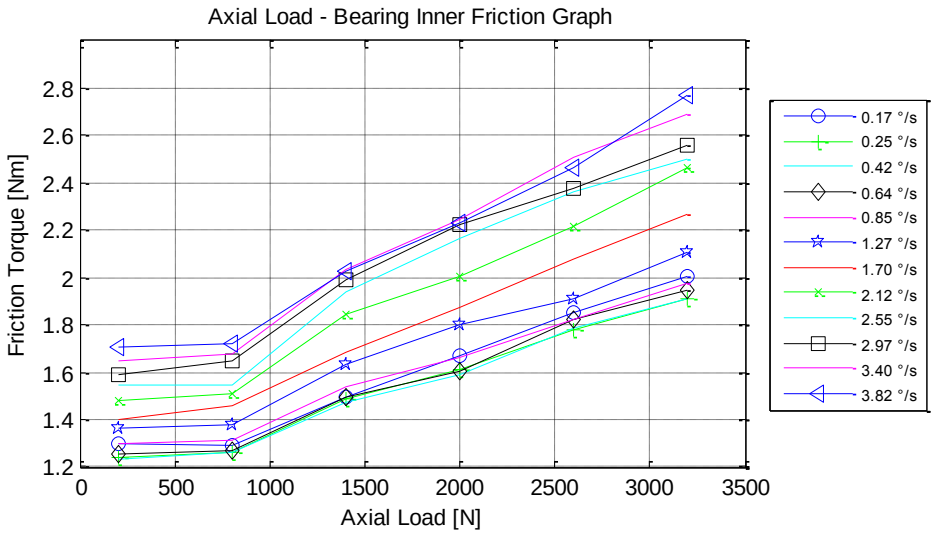

Figure 3.18 Bearing inner friction torque as a function of axial load at different rotational speeds

3.3.4. Bearing Inner Friction Torque in Combined Loading

In order to observe the effect of bearing inner friction torque under combined loading, a tilting moment is applied to the bearing. Figure 3.19 shows the dependence of the friction torque on the tilting moment at 800 N axial loading and at different rotational speeds. The figure presents that as the tilting moment increases, the friction torque increases as well. The increase, however, is not linear. In addition, increase in rotational speed causes friction torque to increase without changing the friction torque profile.

Dependence of the friction torque on the tilting moment at different axial loads is presented in Figure 3.20. At the same rotational speed, increase in tilting moment increases the friction torque. Moreover, increase in axial load increases friction torque.

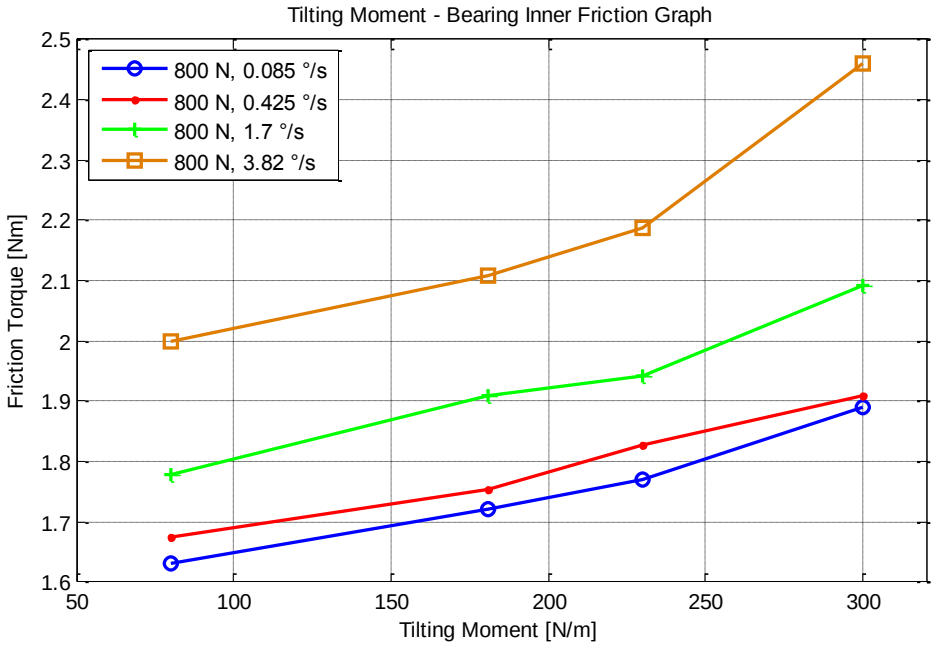

Figure 3.19 Bearing inner friction torque as a function of tilting moment at different rotational speeds

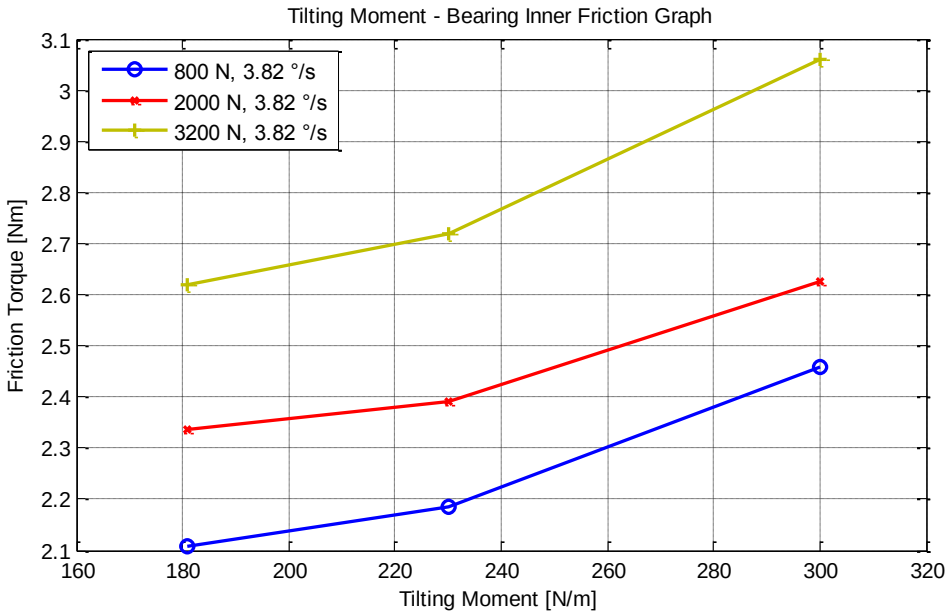

Figure 3.20 Bearing inner friction torque as a function of tilting moment at different axial loads

3.3.5. Upper Seal Friction Torque

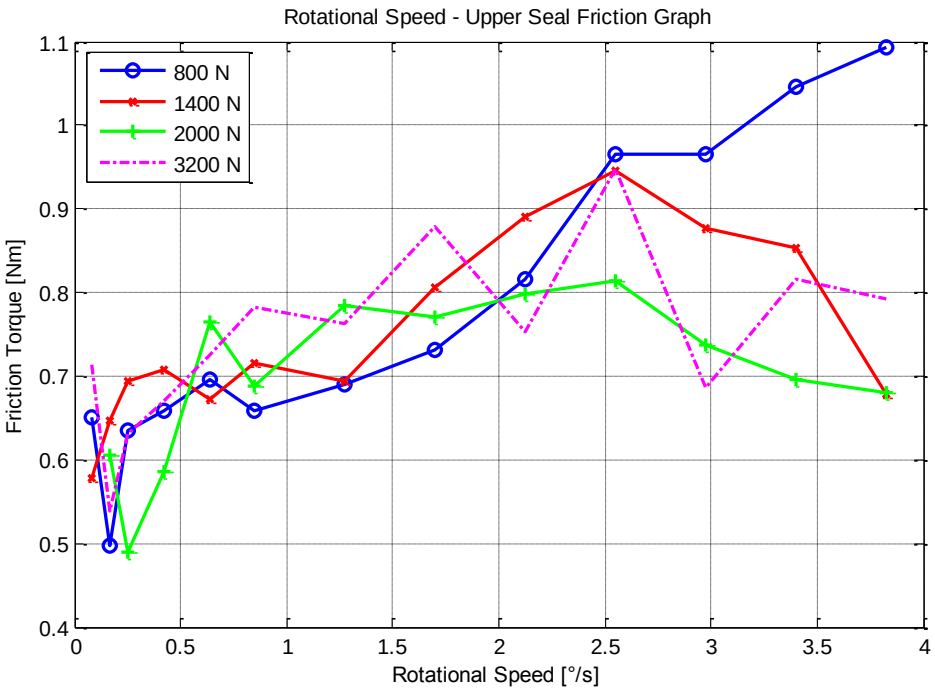

Figure 3.21 Upper seal friction torque as a function of rotational speed at different axial loads

The upper seal friction torque values are presented in Figure 3.21 and 3.22. The upper seal friction torque fluctuates between 0.2 – 1.1 N.m according to speed and load changes. Figure 3.20 presents that, in the same loading conditions, increase in speed causes a slight increase in the friction torque up to rotational speed of 2.5°/s. However, for the speeds which are above 2.5°/s, two different situations occur. For high loads, the friction torque of the upper seal decreases. Conversely, for low loads, the friction torque continues to increase. It can be stated that upper seal friction torque with respect to rotational speed depends also on loading conditions.

In Figure 3.22, the upper seal friction torque with respect to the axial load is given. When the figure is investigated, one conclusion can be drawn: either the effect of load change cannot be observed at this measurement accuracy or the load change is too low to make an effect on the results. Consequently, it can be stated that for working conditions of the slewing bearing, the friction torque due to the upper seal can be taken

as constant. The friction torque at a given speed fluctuates in the range of 0.3 N.m when the load is changed.

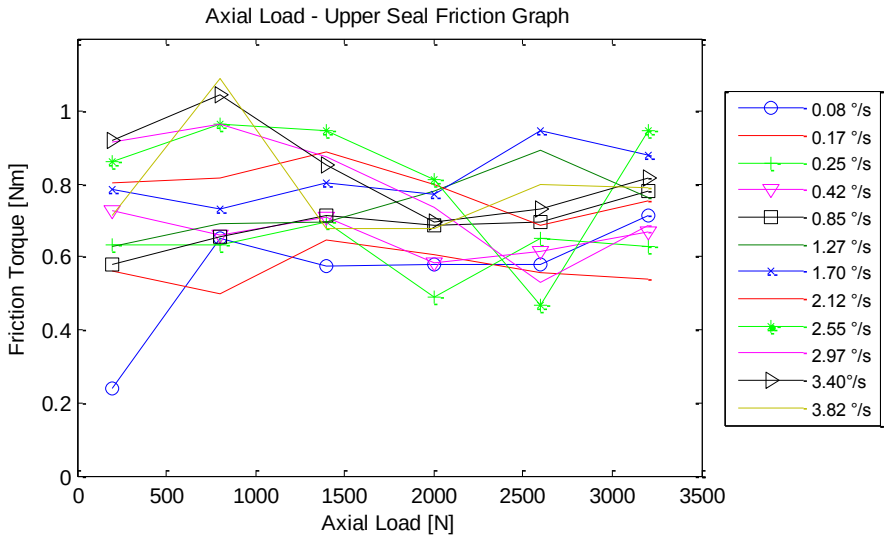

Figure 3.22 Upper seal friction torque as a function of axial load at different rotational speeds

3.3.6. Lower Seal Friction Torque

The lower seal friction torque values are much higher than those of the upper seal friction torque. Figure 3.23 represents the dependence of friction torque on rotational speed in the lower seal. This dependence cannot be defined properly since the trends of friction curves do not match to each other. This may be mainly because of the fact that the change in rotational speed is not high enough to display a difference in lower seal friction.

In Figure 3.24, the effect of variation in load is presented. Increase in load causes a decrease in the lower seal friction torque. This behavior is not expected as in mechanical applications as the load increases, friction increases as well. However, since the lower seal is used with a garter spring, influence of load is different than normal conditions. One possibility is that when load increases, outer ring of the bearing deflects and changes contact area and contact angle between the lower seal and inner ring of the bearing. In addition, deflection in the outer ring may decrease the tension force in the garter spring.

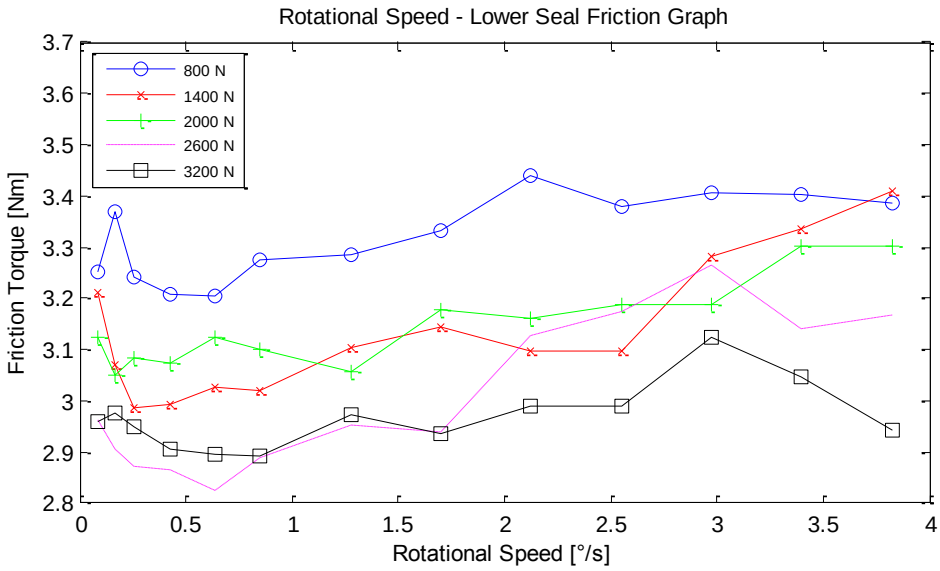

Figure 3.23 Lower seal friction torque as a function of rotational speed at different axial loads

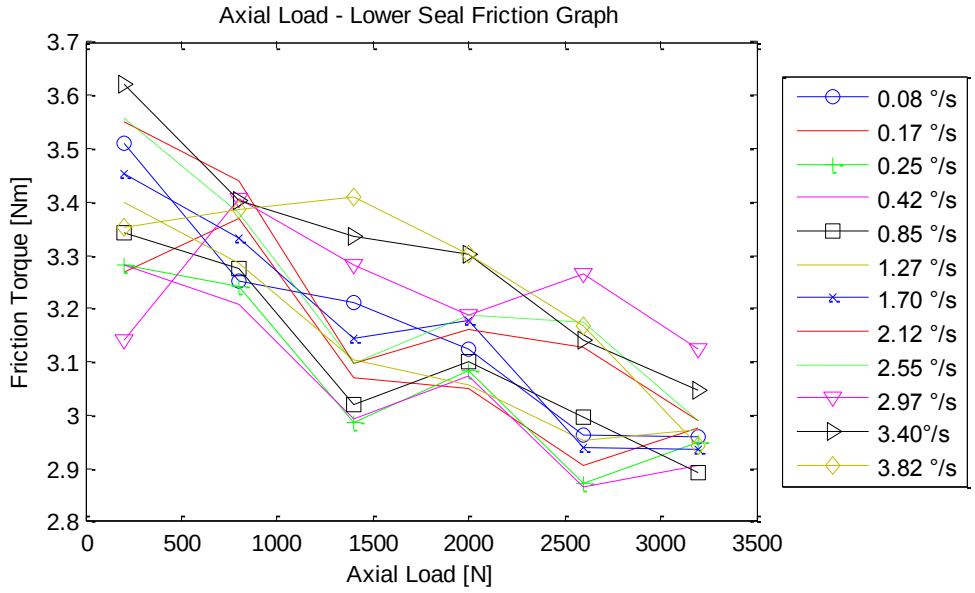

Figure 3.24 Lower seal friction torque as a function of axial load at different rotational speeds

3.3.7. Overview of the Test Results

In order to identify friction torque components of the double row roller slewing bearing, 295 tests are performed at different speeds, loading conditions and configurations. By this way, the effect of loading, rotational speed and causes of friction are determined and analyzed.

According to the test results, following conclusions are drawn:

- Causes of friction are classified as bearing internal mechanism, upper seal and lower seal. According to the test results,
    - 34.5% of total friction is due to the bearing inner mechanism
    - 54.8% of total friction is due to the lower seal
    - 10.7% of total friction is due to the upper seal

  The friction torque caused by sealing elements is 65.5% of total friction of the bearing. Therefore, sealing selection is the most dominant factor affecting the friction torque behavior of the bearing.

- Main cause of inner friction torque of the bearing is associated with the roller-raceway contact. Besides, friction between cages and rollers, and cages and rings may also exist. Nonetheless, in this study, this friction due to the contacts between cages and rollers and cages and rings is ignored. Bearing inner friction torque increases with the increase of both axial load and rotational speed. Moreover, increase in the tilting moment increases friction torque of the bearing as well.
- The contribution by the upper seal friction torque can be said to increase with an increase in rotational speed for low axial loads. However, for high axial loads, friction torque starts to decrease after a specific rotational speed value. Influence of the load on friction torque cannot be determined. This may be mainly because of the fact that the loads are not high enough to make a change in friction torque at the measurement accuracy.
- The contribution by the lower seal friction torque decreases as the axial load increases. This situation can be explained by the change in contact angle and contact area of the lower seal. However, change in rotational speed does not affect friction torque of the lower seal at the measurement accuracy.

CHAPTER 4

FRICTION IDENTIFICATION ANALYSIS

4.1. Friction Analysis Method

Friction torque calculation of the slewing bearing is done by the help of two commercial software namely, ANSYS as a finite element solver and ADAMS as a multibody dynamic simulation program.

Friction torque calculation procedure is given in Figure 4.1. Firstly, the bearing geometry is modeled in ANSYS and loading conditions are defined such as loadings, supports etc. According to the given loadings, ANSYS exports roller/raceway contact forces for each roller. From the results, contact forces are determined and transferred to ADAMS. Secondly, information such as roller and raceway geometry and bearing rotational speed is supplied to ADAMS as inputs. In the end, for a specific loading condition and bearing speed, the corresponding friction torque is calculated by use of user-written friction subroutine. The subroutine considers different lubrication regimes by calculating minimum film thicknesses and friction forces for each step of simulation. Moreover, in order to estimate seal friction torque of the bearing, a simple model for seal friction is generated by exploiting results of the experiments.

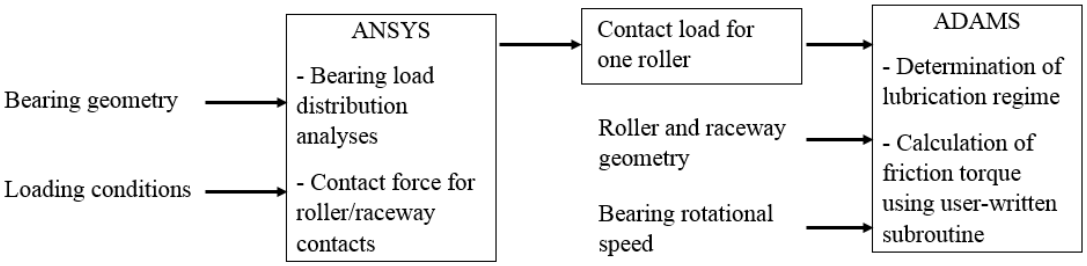

Figure 4.1 Friction Torque Calculation Procedure

4.2. Calculation of Loads on the Slewing Bearing

Slewing bearings can withstand axial loads, radial loads and tilting moments (Figure 4.2). Since the loading affects friction torque of slewing bearings, loads caused by the gun turret should be calculated. In this section, loads acting on the slewing bearing are calculated with the assumption of zero gradients in the turret.

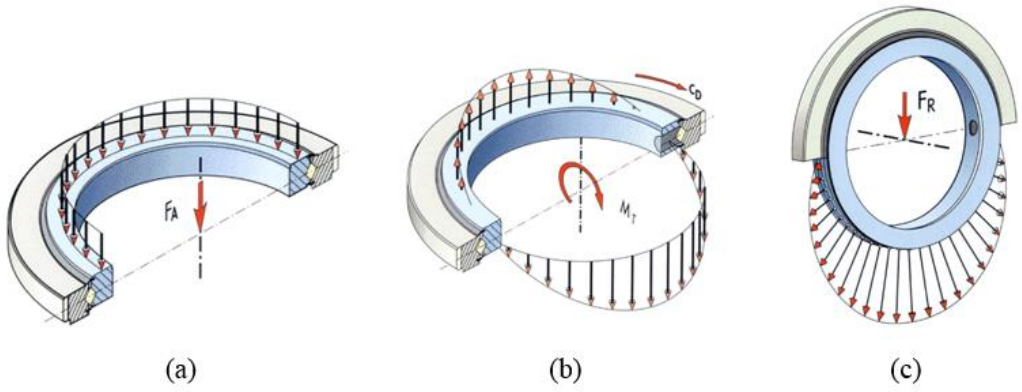

Figure 4.2 Loads acting on a slewing bearing: (a) Axial load, (b) Tilting moment, (c) Radial load (Photo Courtesy of Rollix Inc)

Axial Load: The axial load occurs in the direction of rotation axis of the slewing bearing. The axial load is equal to the total weight of the turret.

$$F_a = \overline{W} \tag{4.1}$$

Tilting Moment: The tilting moment is caused by the distance between the center of mass of the turret and bearing rotation axis.

$$M_t = \bar{W}\sqrt{x'^2 + y'^2} \tag{4.2}$$

Radial Load: The radial load is mainly due to centrifugal force (F_c) and gear force (F_g).

$$F_r = F_c + F_g \tag{4.3}$$

$$F_c = \frac{1}{2} I_{y'y'} \omega^2 \tag{4.4}$$

Force transfer from the electric motor to the turret is provided with a spur gear pair in the slewing bearing. Some of the radial force is due to gear force which can be calculated as [37]

$$F_r = F_t \tan(\bar{\bar{a}}) \tag{4.5}$$

where

$$F_t = \frac{2T}{\bar{d}} \tag{4.6}$$

Forces acting on the bearing are calculated by using Equations (4.1 - 4.6). Parameters used in these calculations are presented in Table 4.1. In calculations, the torque is taken as the maximum torque measured in the tests and rotational speed is taken as the maximum rotational speed in the region of interest.

Table 4.2 summarizes the loads acting on the slewing bearing. According to the results, radial force is very small due to low rotational speed and low friction torque value. So, radial forces will not be considered for friction torque analysis of the slewing bearing.

Table 4.1 Parameters to calculate bearing loads
(Retrieved from documentation of ASELSAN Inc.)

	Parameter	**Value**
Properties of the Turret	$\overline{W}$ [N]	2847
	x' [mm]	55
	z' [mm]	20
	$I_{y'y'}$ [kg.m^2]	37.05
	ω [°/s]	4
Gear Data	d [mm]	480
	$\overline{\overline{\alpha}}$ [°]	20
	T [Nm]	3

Table 4.2 Calculated loads acting on the slewing bearing

Type of Load	Value
F_a [N]	2487
M_t [Nm]	167
F_r [N]	4.5

4.3. Load Distribution of the Slewing Bearing – ANSYS Analysis

Load is transferred from the outer ring to the inner ring by means of rollers. In order to determine the friction force caused by roller – raceway contact, the contact force must be determined. Since combined loading conditions are studied together with axial loads, a finite element program - ANSYS - is used to determine the contact forces between the rollers and raceways.

For the analysis, static structural module of the program is used. In the program, inner and outer rings are modelled. Outer ring is taken as one piece and raceways are integrated into inner and outer rings in order to simplify the geometry. Rollers are

modelled as compression only springs. Seals and cages are not modelled since they do not affect the load distribution on rollers much. The bearing is fixed from the lower face of the inner ring from where the bearing is mounted on one side. The axial load and moment is applied on the upper face of the outer ring. Standard earth gravity is defined in "-y" direction. Finally, a cylindrical support is defined to restrict the rotation of outer ring with respect to the inner ring in "y" direction. Representations of boundary conditions and loadings are given in Figure 4.3.

Model of the slewing bearing is finely meshed and in total 291207 nodal points are used for analysis (Figure 4.4). Solution takes approximately 4 minutes for each loading case on 64-bit computer with 2.4 GHz, 6-core processor. Inner and outer ring materials are taken as aluminum with the specifications given in Figure 4.5.

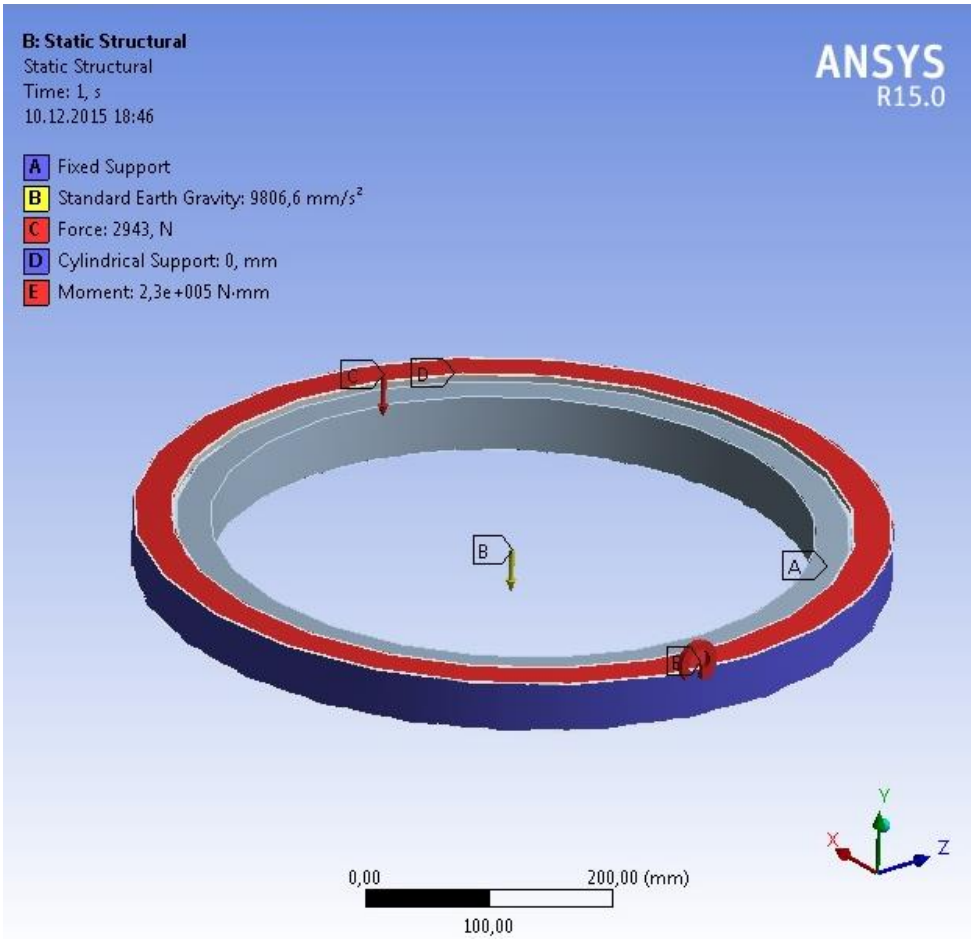

Figure 4.3 Bearing Modeling in ANSYS

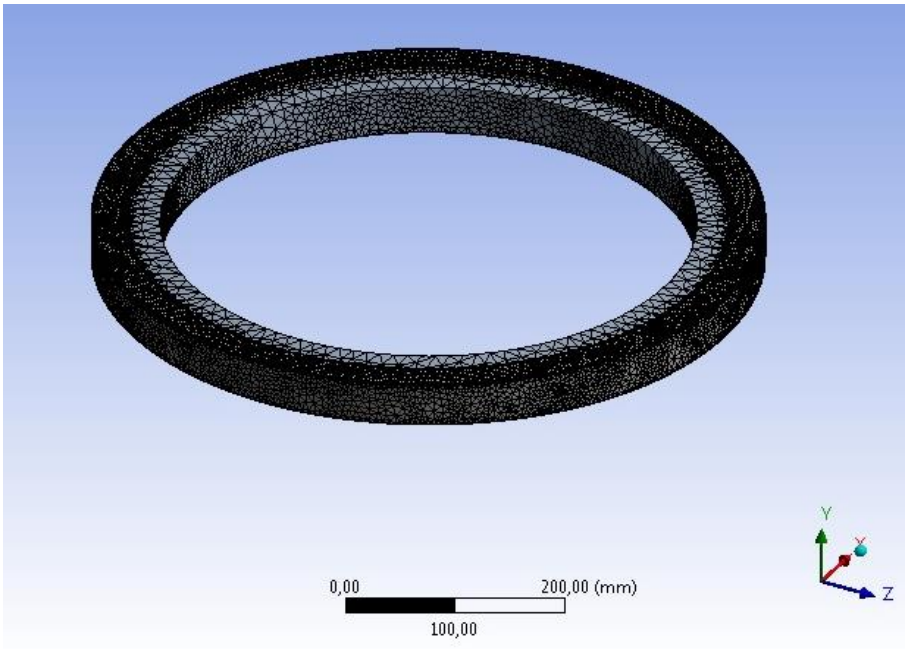

Figure 4.4 Mesh representation of the bearing

Properties of Outline Row 4: Aluminum Alloy 2

	A	B	C	D	E
1	Property	Value	Unit		
2	Density	2820	kg m^-3		
3	Isotropic Secant Coefficient of Thermal Expansion				
4	Coefficient of Thermal Expansion	2,3E-05	C^-1		
5	Reference Temperature	22	C		
6	Isotropic Elasticity				
7	Derive from	Young's Mod...			
8	Young's Modulus	72500	MPa		
9	Poisson's Ratio	0,33			
10	Bulk Modulus	7,1078E+10	Pa		
11	Shear Modulus	2,7256E+10	Pa		
12	Alternating Stress R-Ratio	Tabular			
16	Tensile Yield Strength	370	MPa		
17	Compressive Yield Strength	420	MPa		
18	Tensile Ultimate Strength	3,1E+08	Pa		
19	Compressive Ultimate Strength	0	Pa		

Figure 4.5 Mechanical properties of inner and outer rings

4.3.1. Roller Modelling in ANSYS

Modelling the bearing with all the details causes too long solution times, since it has bunch of elements and contacts between them.

The most critical part to model for the load distribution analysis is the rollers. Rollers make contact with the inner and outer rings transferring the force between them. So, in the finite element analysis program, rollers are modeled as compression only springs. Spring constants are calculated as given in [38].

$$F_n = K_1 \delta_m \tag{4.7}$$

where

$$K_{1,x} = \frac{\pi l E'}{2[\frac{2}{3} + \ln\left(\frac{2d_{1,x}}{b_x}\right) + \ln\left(\frac{2d_2}{b_x}\right)]} \tag{4.8}$$

$$\delta_m = \delta_{mo} + \delta_{mi} \tag{4.9}$$

Equation (4.8) consists of x subscripts which can be chosen as "i" or "o" meaning inner and outer diameters, respectively. Half width of the contact area, "b" is calculated by Hertz theory [37].

$$b_x = \sqrt{\frac{2F}{\pi l} \frac{(\frac{1-v_1^2}{E_1}) + (\frac{1-v_2^2}{E_2})}{\frac{1}{d_{1,x}} + \frac{1}{d_2}}} \tag{4.10}$$

In the calculations, variables used for the slewing bearing are displayed in Table 4.3.

By the use of equations (4.8) and (4.10), the contact stiffness values between roller-inner raceway and roller-outer raceway are calculated for different force values ranging between 0 - 450 N. Total deflections occurring in the inner raceway – roller contact and the outer raceway –roller contact with respect to the applied force is given in Figure 4.6. From the slope of force-deformation curve, contact stiffness is calculated as 53000 N/mm.

The method of modeling rollers as springs is used by several researchers and reported to be as a good approximation [39] [40].

Table 4.3 Variables used for contact stiffness

Variable	**Value**
l [mm]	5.2
E_1 $[GPa]$	203
E_2 $[GPa]$	201.5
v_1	0.24
v_2	0.28
$d_{1,i}$ [mm]	540,88
$d_{1,o}$ [mm]	563,5
d_2 [mm]	8

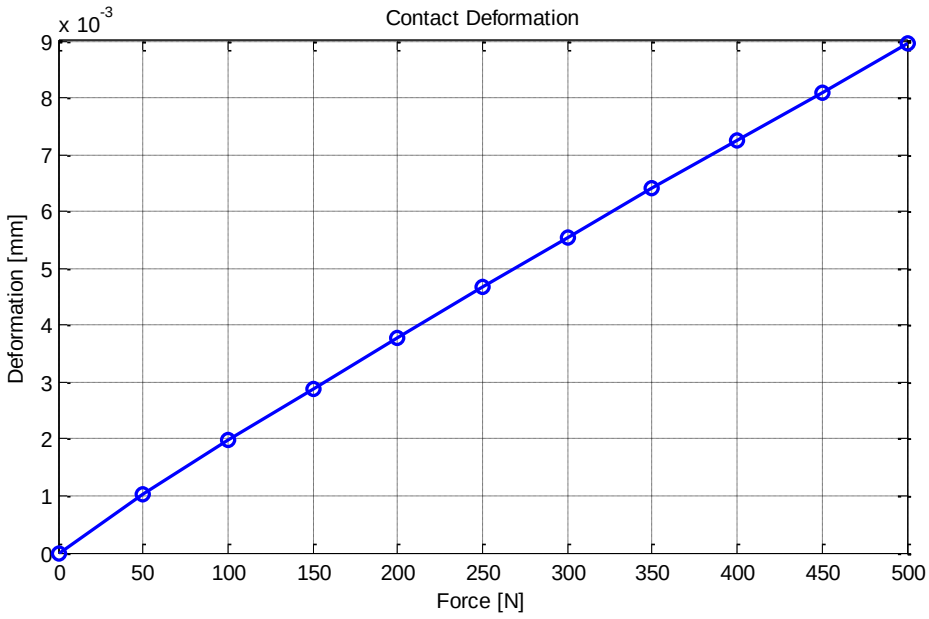

Figure 4.6 Inner raceway - roller - outer raceway contact deformation as a function of contact force

In ANSYS, springs are modelled as compression only springs, since no tensile force is applied onto the rollers between raceways due to contacts. The only viable force applied to the roller is the compression force. In order to simulate this effect, stiffness is imported in the form of tabular data as shown in Figure 4.7. When a negative deflection occurs in the spring, it applies a compressive force. However, when the spring length increases - meaning positive deflection occurs-, no force is applied at the contact. In order to make the solver converge to a solution, a negligibly small value of force is used (i.e. 100 N for 1 mm deflection).

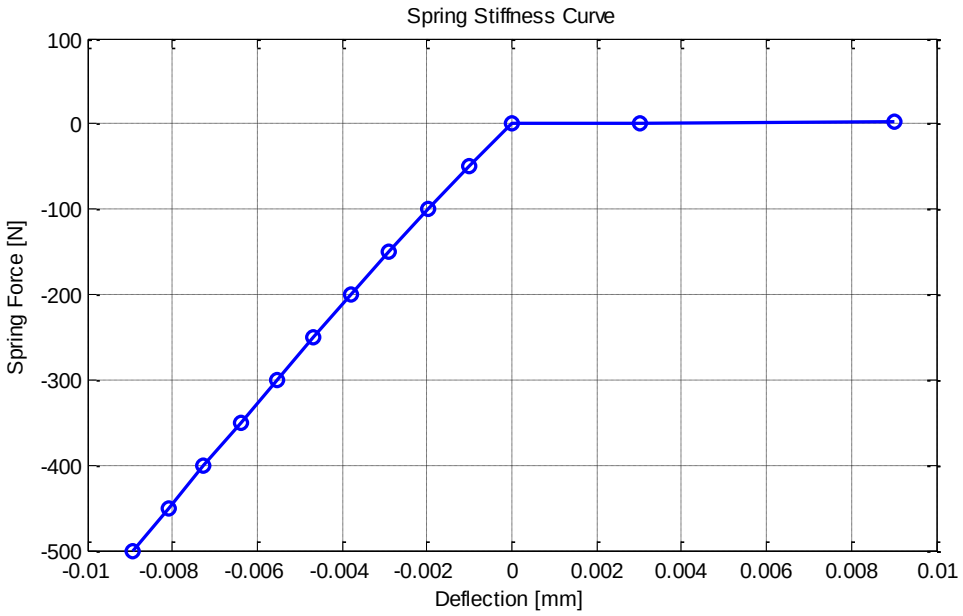

Figure 4.7 Compression only spring model

In total, 290 springs are connected equidistantly between the inner and outer raceways. (Figure 4.8) Then, axial and tilting moment loadings are applied to the bearing to obtain roller contact forces. Analyses are performed according to the test procedure given in Chapter 3. Two different types of analyses are done as

- Pure Axial Loading Analysis
- Combined Loading Analysis

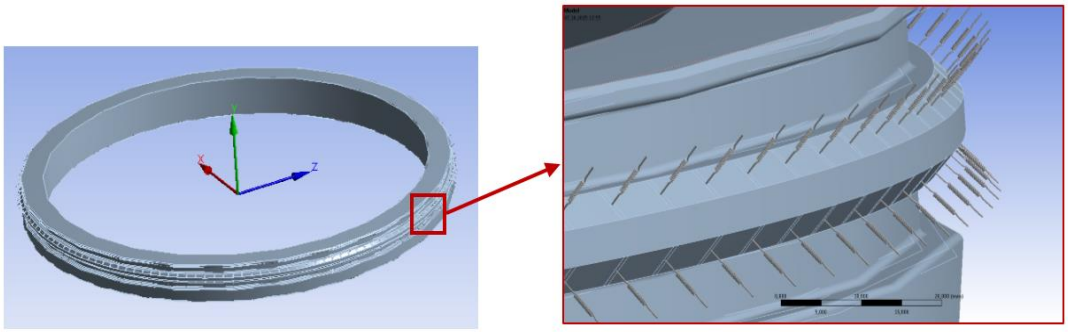

Figure 4.8 Spring models in ANSYS

4.3.2. Load Distribution Analysis Results

In the pure axial loading analysis, it's been observed that the load is distributed among the rollers located in the upper row. No force is exerted on the rollers located in the lower row, since all the load is supported by the rollers in the upper row. Table 4.4 presents contact force and deflection data of the rollers in the upper and lower rows. As expected, increase in axial load causes increases in contact force and deflection.

Table 4.4 Contact force and deflection data of rollers

	Upper Row Rollers		**Lower Row Rollers**	
Axial Load (N)	**Contact Force (N)**	**Deflection (mm)**	**Contact Force (N)**	**Deflection (mm)**
0	-0.57365	-1.08E-05	4.62E-03	4.62E-05
800	-8.3315	-1.57E-04	6.97E-02	6.97E-04
1200	-11.925	-2.25E-04	0.10009	1.00E-03
1800	-17.603	-3.32E-04	0.1479	1.48E-03
2400	-23.278	-4.39E-04	0.19573	1.96E-03
3000	-28.959	-5.46E-04	0.24364	2.44E-03

In combined loading analysis, the situation differs from the pure axial loading case. When a moment is introduced to the system, according to the direction of moment load, more force is exerted on the rollers on one side of the bearing compared to the other side. This configuration is presented in Figure 4.9. Load distribution circles shift

to the up because of the tilting moment. In addition, it can be seen that increase in axial load causes increases in the radius of load profile.

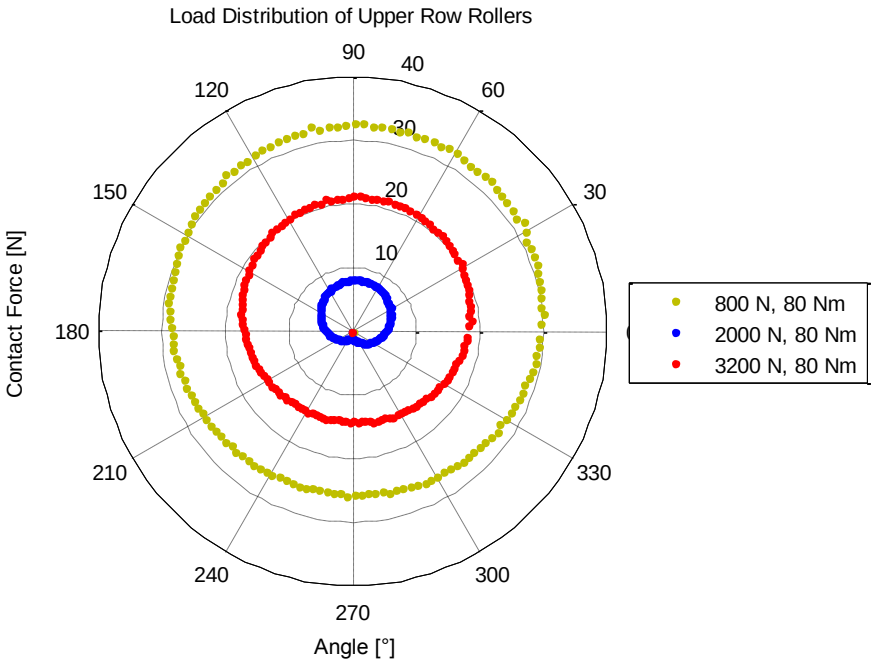

Figure 4.9 Load distribution of upper row rollers at different axial loads

Figure 4.10 shows the change in load distribution of upper row rollers with respect to a change in tilting moment while keeping the axial load constant. As the tilting moment increases, load distribution shifts to one side of the bearing. (Direction of tilting moment is from 0° to 180°)

If the tilting moment increases such that in one side of the bearing it overcomes the effect of axial load, lower row rollers starts to be compressed and upper row rollers are relieved. Load distribution of upper and lower rollers for an axial load of 800 N and a tilting moment of 300 Nm is given in Figure 4.11. It can be observed that for upper row rollers, the moment and axial load act in the same direction, so higher roller loads are obtained in the upper row.

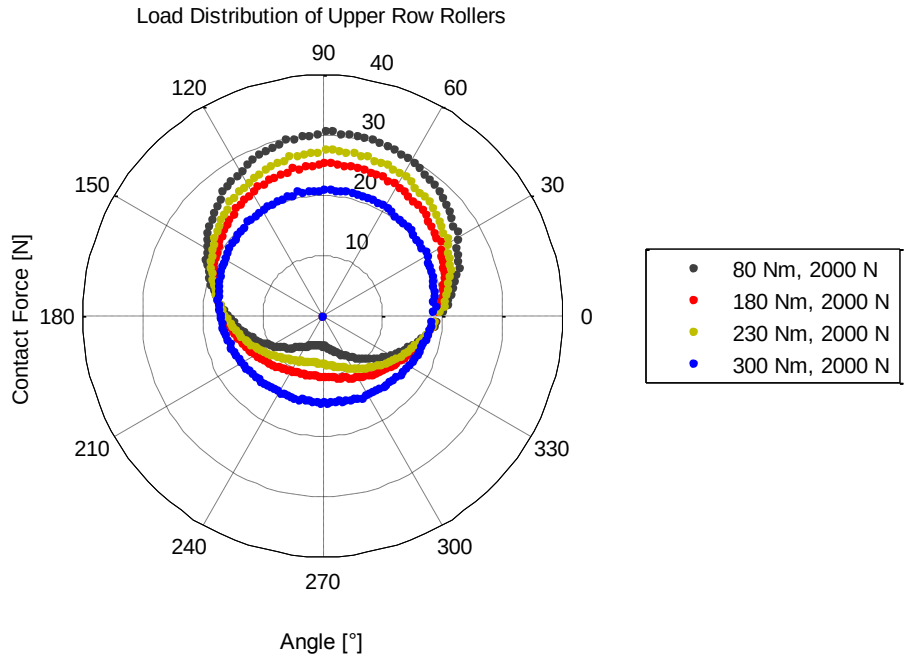

Figure 4.10 Load distribution of upper row rollers at different tilting moments

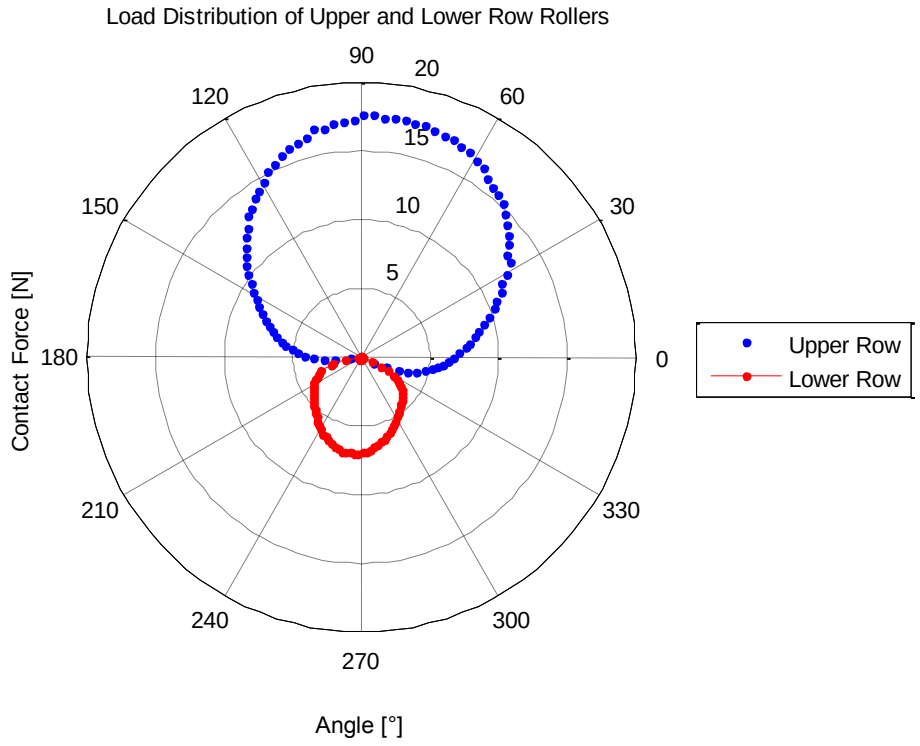

Figure 4.11 Load distribution of upper and lower row rollers
(Axial Load = 800 N, Tilting Moment = 300 Nm)

4.4.Friction Identification Analysis – ADAMS Analysis

As mentioned before, in order to identify friction force during motion, a multibody dynamic simulation program called ADAMS is used. In ADAMS, a basic raceway and roller model is generated. The roller model is taken from 3D drawings of the bearing. Raceways are generated as boxes while keeping raceway widths same as the bearing raceway. Both raceways and rollers are modelled as steel.

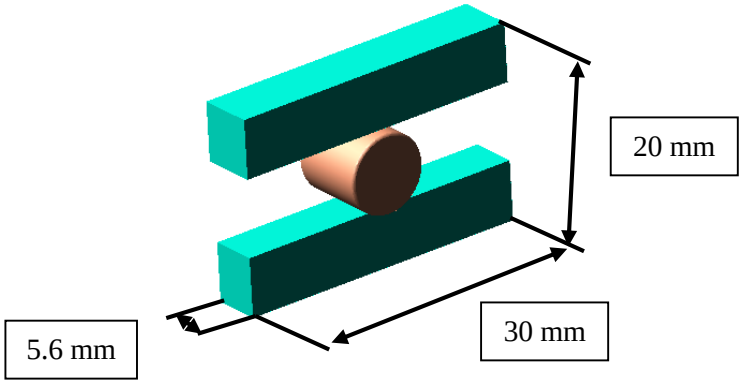

Figure 4.12 Roller – raceway model

Boundary conditions used in the model are given below:

- Lower box is fixed to the ground.
- Contact force is defined between roller and raceways.
- Force is applied from the upper box perpendicular to the upper box surface.
- For the upper and lower boxes to move parallel to each other, a parallel joint primitive is defined.
- Constant speed motion is imposed to the upper raceway in the longitudinal direction.

4.4.1. Contact Force Modelling in ADAMS

There are two contact force models in ADAMS: Poisson model and impact model. Both models use a penalty regularization of the normal contact constraints. In Poisson

model, contact force is calculated with two variables which are penalty value and restitution coefficient. Poisson model is a simpler model; however model parameters are not physically interpreted values, so choice of the right parameter value depends on the experience of the analyst. Impact model however, requires four different parameters such as contact stiffness, force exponent, damping and penetration depth.

In the analysis, the impact model option of ADAMS is used as the contact force calculation method (Figure 4.13). The stiffness value, which is calculated in Section 4.3.1, is taken as 106000 N/mm. The force exponent is taken as 3, the damping coefficient is 10 Ns/mm and the penetration gap is determined as 0.01 mm. These three values are determined with the help of ADAMS' help documentation, and the trial and error method for the analysis.

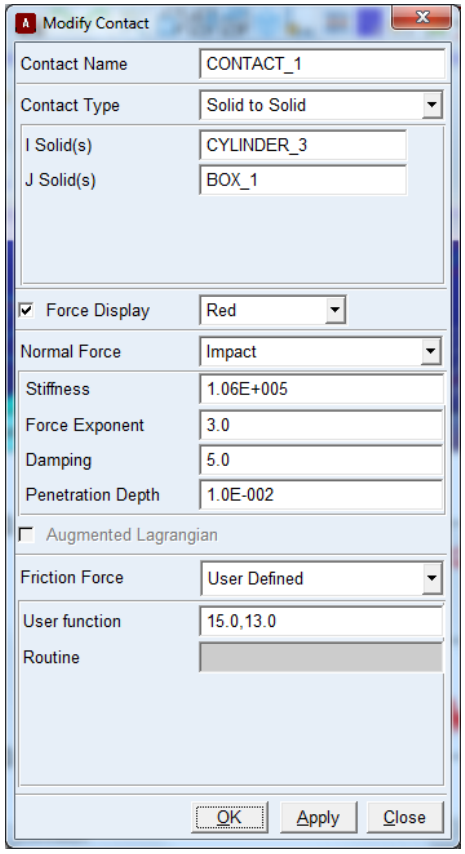

Figure 4.13 Contact force dialog box

When defining contact force, friction force model should be selected too. The program lets users to choose Coulomb Friction only. However, as test results suggest, Coulomb

Friction is not applicable in this case, since the friction coefficient is not directly proportional to contact force. Moreover, the friction force is also dependent on the slip velocity of surfaces. So, a user-written friction force subroutine is coded in FORTRAN by using the models in Sections 4.4.2 and 4.4.3 and implemented to ADAMS. Friction subroutine is given in Appendix A-1.

4.4.2. Determination of Lubrication Regime - Theory

In order to model a bearing dynamically, traction forces must be investigated. Since the bearings are lubricated, traction forces may change according to the lubrication regimes. In literature, four different types of lubrication regimes for line contacts are defined as rigid solid - isoviscous (RI), elastic - solid isoviscous (EI), rigid solid - piezoviscous (RV) and elastic solid - piezoviscous.

Winer and Chang [41] suggested dimensionless viscosity parameter (g_v) and dimensionless elasticity parameter (g_e) to define lubrication regime of a contact.

$$g_v = \left(\frac{a^2 w_l^3}{\eta_0 \mathrm{R}^2 \mathrm{u}}\right)^{0.5} = \left(\frac{G^2 W^3}{U}\right)^{0.5} \tag{4.11}$$

$$g_e = \left(\frac{w_l^2}{\eta_0 \mathrm{E}' \mathrm{Ru}}\right)^{0.5} = \left(\frac{W^2}{U}\right)^{0.5} \tag{4.12}$$

where

$$G = a\, E' \tag{4.13}$$

$$U = \frac{\eta_0 u}{E' R} \tag{4.14}$$

$$W = \frac{w_l}{\mathrm{E}' \mathrm{R}} \tag{4.15}$$

According to calculated g_v and g_e parameters, lubrication regime of the contact can be determined using the lubrication regime map given by Khonsari and Kumar. [42]

In Figure 4.14, there are shaded areas that the lubrication regimes are not strictly defined. For the boundaries of regimes, a mean line of the shaded areas can be used [43].

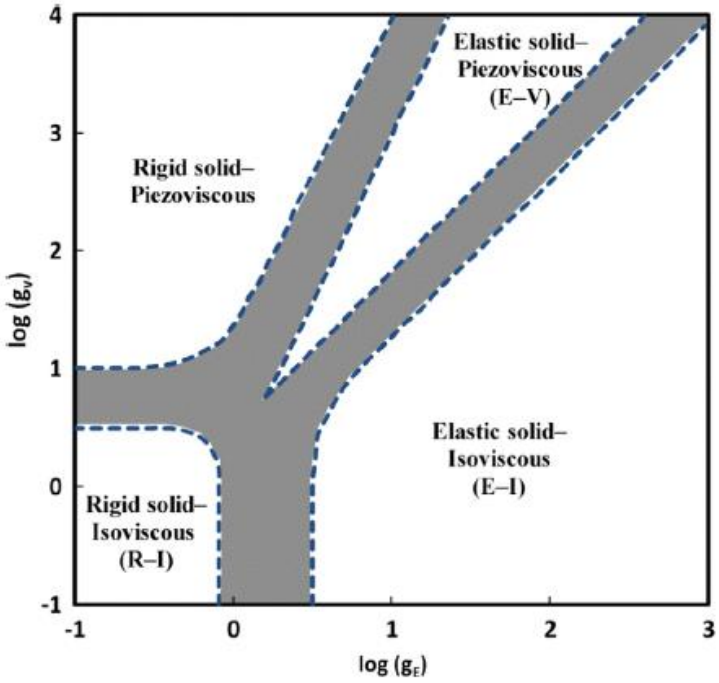

Figure 4.14 Lubrication regimes of line contacts [42]

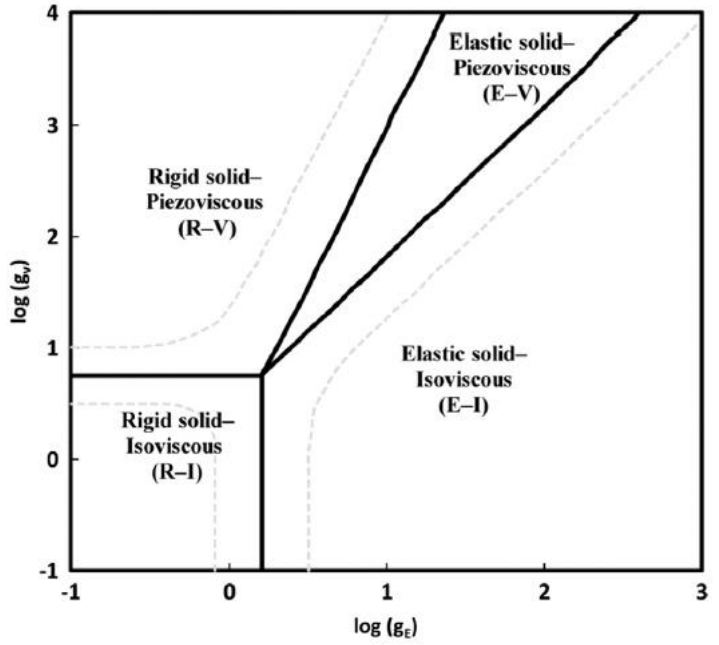

Figure 4.15 Modified regimes of lubrication for line contacts [43]

Rigid Solid – Isoviscous Lubrication Regime (RI)

In rigid solid – isoviscous lubrication regime, viscosity of the lubricant does not change since contact pressure is low. In addition, no elastic deformation is observed in this regime. Since the pressure is insignificant, dimensionless film thickness parameter is taken as constant. [41], [42]

$$h' = 4.9 \tag{4.16}$$

$$h' = \frac{h_{min} w_l}{\eta_0 \mathrm{Ru}} \tag{4.17}$$

In order to calculate the traction coefficient, shear stress can be calculated as

$$\tau = \eta \frac{u_s}{h_{min}} \tag{4.18}$$

In this equation, viscosity is taken as the inlet viscosity at atmospheric pressure.

Elastic Solid – Isoviscous Lubricaiton Regime (EI)

In this regime, elastic deformation of the solids exists. However, the lubricant pressure does not change much. Dimensionless film thickness can be calculated as [41], [42]

$$h' = 0.3\, g_E^{0.8} \tag{4.19}$$

Minimum film thickness and shear stress can then be calculated by Equations 4.17 and 4.18, respectively. In Equation 4.18, viscosity at atmospheric pressure is to be used.

Rigid Solid – Piezoviscous Lubrication Regime (RV)

In this regime, pressure is assumed to be high enough to affect lubricant's viscosity; however, the solid is not exposed to elastic deformation [44]. Dimensionless film thickness can be calculated as [41], [42]

$$h' = 1.66\, g_v^{2/3} \tag{4.20}$$

Since the pressure is assumed as high enough to change the viscosity of lubricant, viscosity under pressure should be calculated by using Roelands pressure-viscosity relationship. [45], [46]

$$\frac{\eta}{\eta_0} = \exp\{(ln(\eta_0) + 9.67)x[-1 + (1 + 5.1x10^{-9}p_h)^{z_1}]\} \quad (4.21)$$

$$z_1 = \frac{a}{5.1x10^{-9}(\ln(\eta_0) + 9.67)} \quad (4.22)$$

Minimum film thickness and shear stress can then be calculated by using equations 4.17 and 4.18, respectively.

Elastic Solid – Piezoviscous Lubrication Regime (EV)

In EV, pressure is much higher compared to other regimes. Consequently, elastic deformation of the solids becomes higher and viscosity of the lubricant increases. For dimensionless film thickness, the following formula can be used [41]:

$$h' = 2.65\ g_v^{0.5}\ g_E^{0.06} \quad (4.23)$$

The shear stress can be calculated by using Equations 4.21, 4.22, 4.17 and 4.18. However, in elastic solid – piezoviscous lubrication regime effect of surface roughness should be implemented into the model. Masjedi and Khonsari investigated traction coefficient in line-contacts considering surface roughness and hardness. They give traction coefficient formula as [47]

$$f = \frac{F_f}{F_n} = \left(\frac{L_a}{100}\right) f_c + \frac{2bl\tau_{lim}}{F_n}\left(1 - \exp\left(-\frac{\eta u_s}{\tau_{lim} h_c}\right)\right) \quad (4.24)$$

where

$$h_c = 2.691W^{-0.135}U^{0.705}G^{0.556}R[1 + 0.2\bar{\sigma}^{1.222}V^{0.223}W^{-0.229}U^{-0.748}G^{-0.842}] \quad (4.25)$$

$$h_{min} = 1.652W^{-0.077}U^{0.716}G^{0.695}R[1 + 0.026\bar{\sigma}^{1.12}V^{0.185}W^{-0.312}U^{-0.809}G^{-0.977}]$$

$$L_a = 0.005W^{-0.408}U^{-0.088}G^{0.103}[\ln(1 + 4470\bar{\sigma}^{6.015}V^{1.168}W^{0.485}U^{-3.741}G^{-2.898}]$$

$$\tau_{lim} = \Lambda_{lim} p_h = \Lambda_{lim}.p(1 - \frac{L_a}{100})$$

The minimum film thickness values are calculated for given load and speed values by using the methods explained above. After calculating minimum film thickness, the film parameter is calculated as [38]

$$\Lambda = \frac{h_{min}}{\sqrt{R_{ro}^2 + R_{ra}^2}} \tag{4.25}$$

According to the film parameter calculated, the friction coefficient can be decided according to the information given below [28], [48].

$$\mu = \begin{cases} \mu_{bd} & if \quad \Lambda < 1 \\ \dfrac{\mu_{bd} - \mu_{hd}}{(\Lambda_b - \Lambda_h)^6}(\Lambda - \Lambda_h)^6 + \mu_{hd} & if \quad 1 < \Lambda < 5 \\ \mu_{hd} & if \quad 5 < \Lambda \end{cases} \tag{4.26}$$

μ_{bd} is determined by test results. Because, the effect of lubrication is minimized and no proper model is found for this region. Determination of the friction coefficient from test results is explained in Section 4.4.3. In the case where Λ is higher than 5, hydrodynamic friction coefficient is calculated by using Equations 4.16-4.22. In the intermediate region, effects of both hydrodynamic and boundary lubrication are observed. Sakaguchi et al. introduced a convergence formula to predict the friction coefficient in this region [48].

4.4.3. Traction Force in the Boundary Lubrication Regime

For the boundary lubrication regime, friction force is modelled by curve fit data of test results. From constant speed and constant axial load data, friction force is curve fitted as

$$F_{friction} = (0.0315\mathrm{F_{ct}} + 0.0979)\omega + 0.0288F_{ct} + 1.062 \tag{4.27}$$

where F_{ct} is roller/raceway contact force in Newton, ω is bearing rotational speed in °/s.

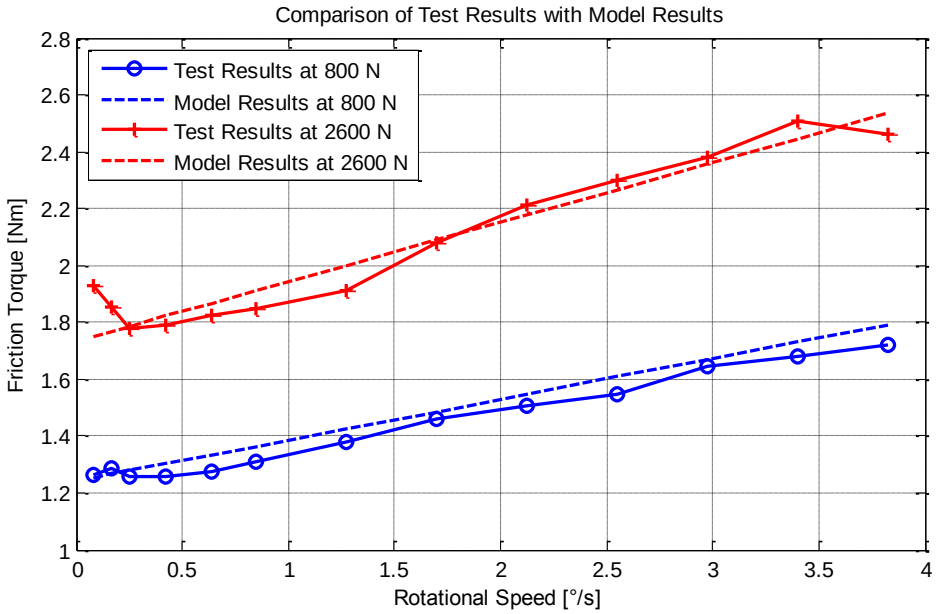

Figure 4.16 Comparison of test results with model results

Frictional model obtained from test results is implemented into the user developed-subroutine as the friction force in boundary lubrication regime.

4.4.4. Calculation Method for Bearing Friction Torque

Firstly, pure axial loading analyses are performed. Since the only loading is axial load, rollers in the upper row are loaded equally. So, simulations are performed for one roller only and the result is multiplied with the number of rollers in the upper row. In Figure 4.17, a sample simulation result is presented for axial load of 3200 N and speed of 2.15 °/s. For this example, the friction is calculated as 0.055 N. Multiplying this value with bearing mean radius and number of rollers gives the friction torque of the bearing as 2.2 Nm.

Secondly, tilting moment analyses are performed. Contrary to the pure axial loading, in tilting moment condition, roller loads are different from each other. In order to determine the friction force, roller forces are applied to one roller at each time step. In order to do so, force input is given as a function representing all roller loads instead of a constant value. In tilting moment analysis, the maximum torque value is taken as the friction torque of the bearing. In Section 4.5, results of the analysis are compared with test results.

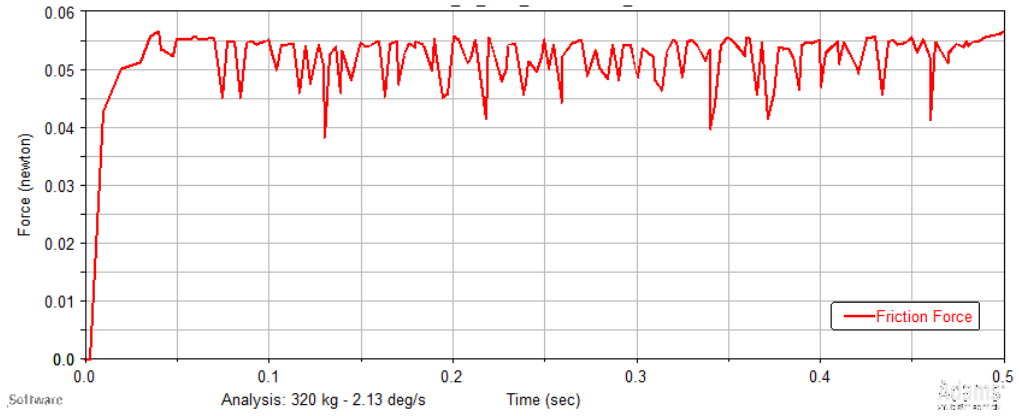

Figure 4.17 Sample Simulation Result (Load = 3200 N, Speed=2.15 °/s)

4.5. Results of the Analysis

4.5.1. Axial Loading Analysis Results

The axial loading analyses are performed for axial loads of 800 N, 2000 N and 3200 N. Each analysis is run for 13 different rotational speeds. In Figure 4.18, the change in bearing friction torque is illustrated with respect to rotational speed for both test and analysis results. Analysis and test results fit with a maximum error of 6%. This difference may be caused by the choice of contact parameters in multibody dynamic simulation program. Some of the contact parameters such as force exponent, damping and penetration depth are determined with trial and error method. General trend for analysis results is that, analyses overestimate test results with a small difference.

4.5.2. Tilting Moment Analysis Results

Tilting moment analyses are performed for four different tilting moment values such as 80 Nm, 180 Nm, 230 Nm and 300 Nm; for three different axial loading values such as 800 N, 2000 N and 3200 N; and for four different rotational speeds such as 0.085°/s, 0.425°/s, 1.7°/s and 3.82°/s.

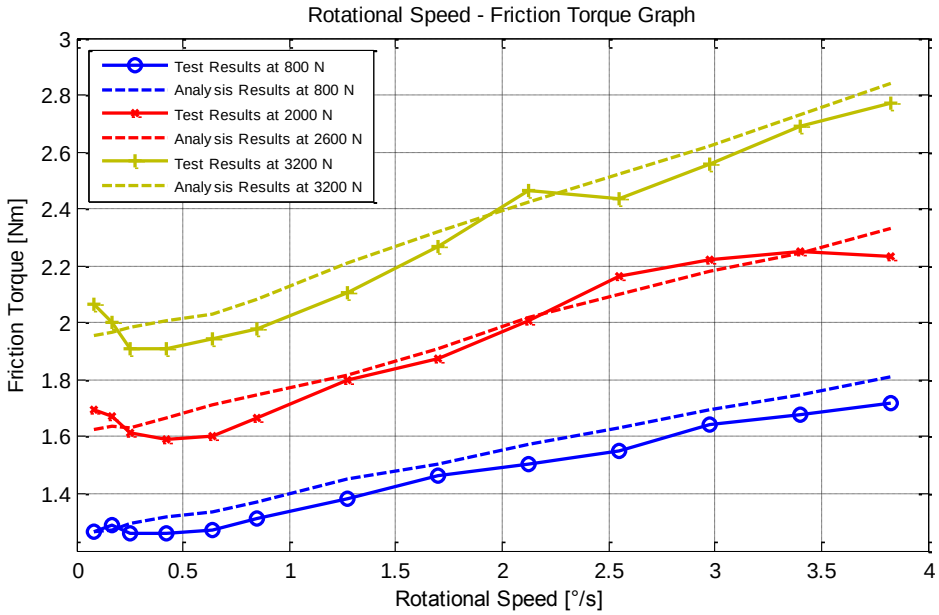

Figure 4.18 Comparison of analysis and tests in axial loading

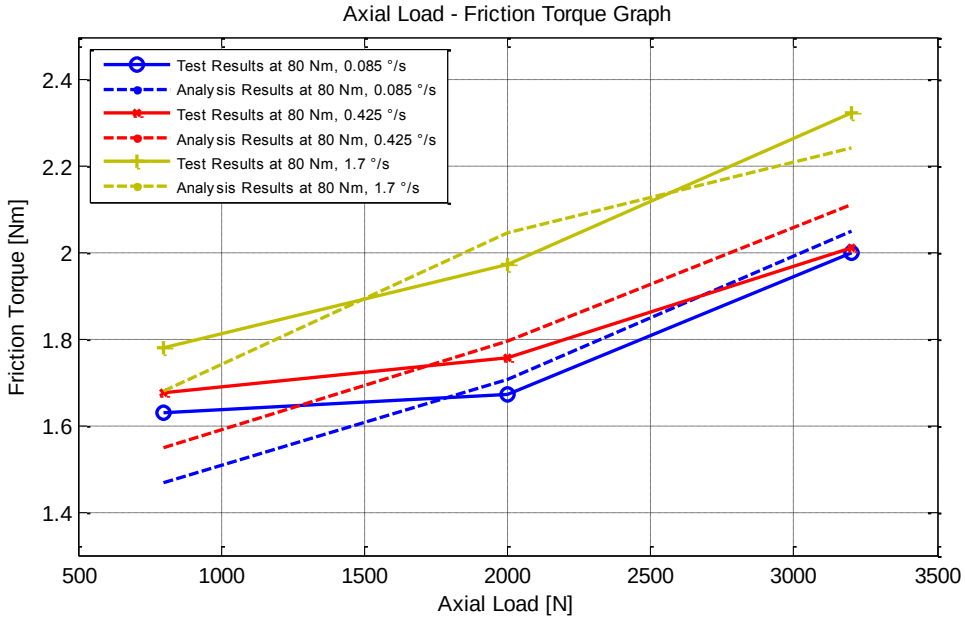

Figure 4.19 Comparison of analysis and test results – effect of axial load

In Figure 4.19, comparison of analysis and test results at 80 Nm tilting moment is displayed with respect to changes in axial load. As axial load increases, the friction torque increases as well for both analysis and test results. According to the test results, increase in the friction torque from axial load of 800 N to 2000 N is lower than the increase from axial load of 2000 N to 3200 N. However, such trend is not observed for analysis results. The reason may be attributed to that at low axial loads, the friction torque prediction is not accurate enough. Maximum discrepancy between the results of test and analysis is 0.16 Nm at low axial loads which corresponds to 10% of total value. When the axial loading increases, maximum error decreases down to 4%, which means accuracy of the model increases with the increase in axial load.

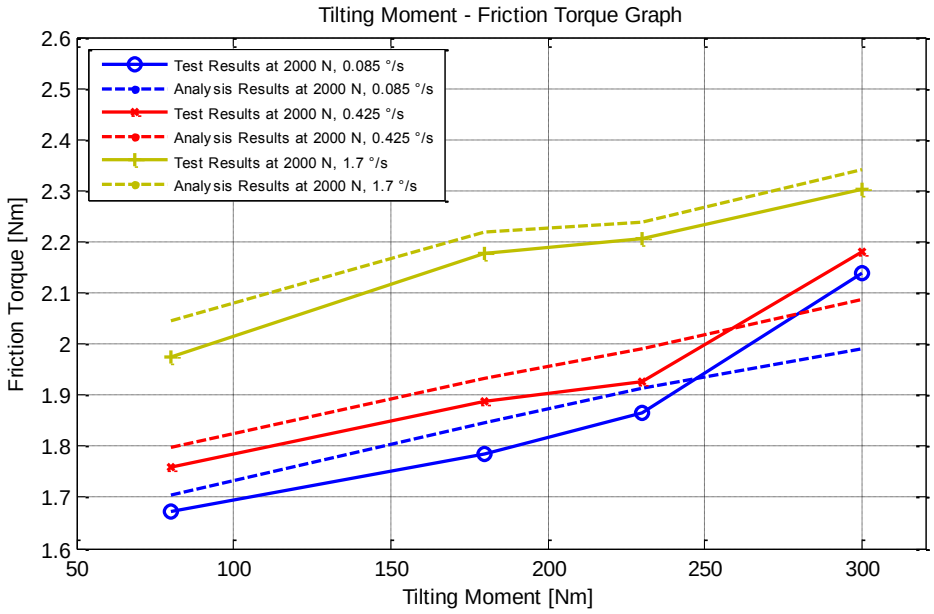

Figure 4.20 Comparison of analysis and test results – effect of tilting moment

Figure 4.20 represents the comparison of the analysis and test results of the friction torque at an axial load of 2000 N with respect to changes in tilting moment. In the comparison, The maximum error of 7% occurs at the highest tilting moment value – 300 Nm. Curves are in increasing trend for both test and analysis results. Increase rate of friction torque obtained from tests between 230 Nm to 300 Nm is much higher than the increase rate of analysis result.

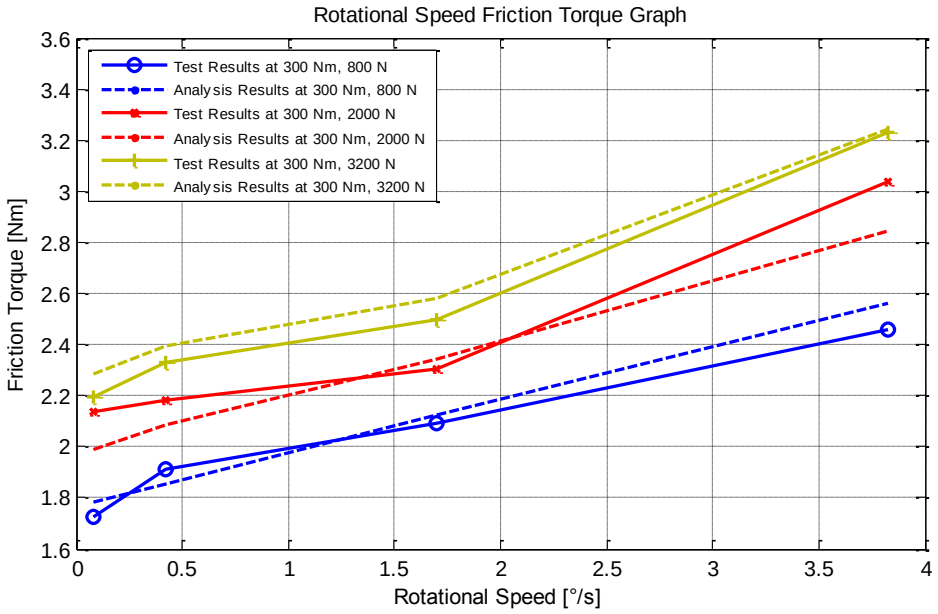

Figure 4.21 Comparison of analysis and test results – effect of rotational speed

In Figure 4.21, the influence of rotational speeds on friction torque is investigated at tilting moment of 300 Nm for three different axial loads. Both the test and analysis results have the same tendency that an increase in rotational speed causes increase in friction torque. The maximum error of 0.19 Nm is obtained at the highest and lowest speed values.

4.5.3. Seal Friction Analysis Results

There exist two lip seals in the slewing bearing. The upper seal is used in the inner part of the slewing bearing while the lower seal is employed in the outer part of the slewing bearing where harsh environmental conditions exist. So, the lower lip seal is used with a garter spring in order to increase the contact force between the seal and outer ring of the bearing.

In Chapter 3, the friction torque values of upper and lower seals are experimentally obtained with respect to different speed and loading conditions. According to the test results, the effect of load and speed on the upper seal friction torque cannot be observed. The reason could be attributed to the fact that the change in load and speed is not high enough to observe any difference at the measurement accuracy of the test

setup. So, for the analysis point of view, it will not be a wrong approach to accept the friction torque of upper seal as constant and this value is the average value of test results. For linear speeds between 0.4 mm/s and 18.4 mm/s and for loadings up to 3200 N, upper seal friction torque can be accepted as 0.7 Nm with a maximum error of 0.4 Nm.

For the lower seal, any effect of speed change cannot be observed as for the case of upper seal. However, the effect of loading is definite. As the load increases, the friction torque of the lower seal decreases and this effect can be approximated linearly as

$$T_{friction} = -0.00016F_a + 3.43 \tag{4.28}$$

where F_a is axial loading in N, and $T_{friction}$ is given in Nm.

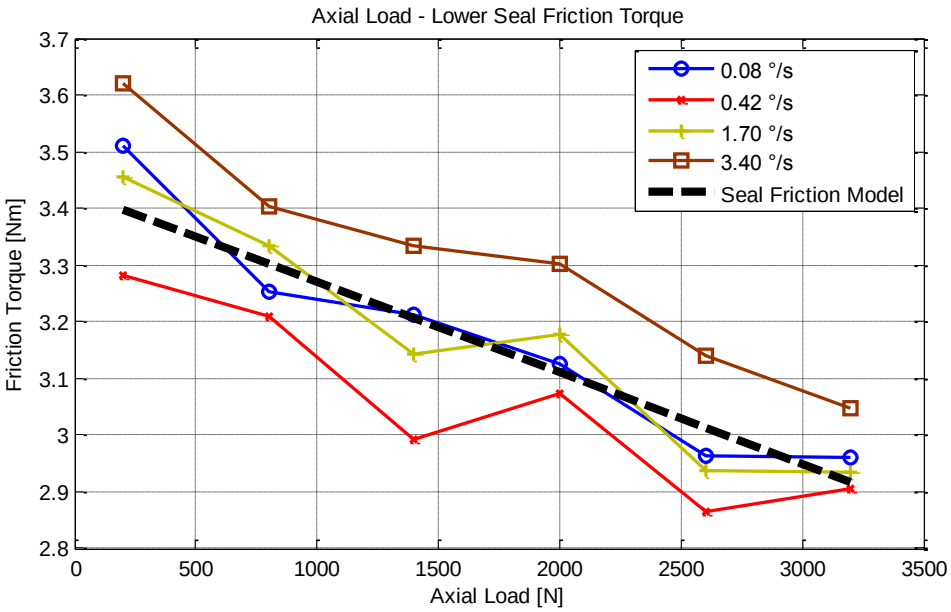

Figure 4.22 Comparison of analysis and test results – lower seal friction torque

In figure 4.22, comparison between the analysis and test results for the lower seal friction torque is presented. Equation 4.28 is valid for linear speeds in the range of 0.4 mm/s and 18.4 mm/s and for loadings up to 3200 N with a maximum error of 0.25 Nm.

CHAPTER 5

SUMMARY AND CONCLUSIONS

5.1. Summary

Friction is always an important subject for mechanical systems. Although there are some applications which requires friction force such as vehicle brakes, clutches and tires, friction is generally viewed as an energy consuming and useless force against motion. As friction force is always against motion, it affects the stability of motion as well. Therefore, designs of components and systems are made in a way to reduce friction in order to conserve energy and to have a stable motion.

Gun turret systems, which are called as stabilized gun platforms, require stable motion in order to follow targets accurately. The most important destabilizing factor of gun turrets is the friction occurring at low speeds. Main reason for the friction is the bearings used in rotation axes of the turret. In this thesis, investigation of the slewing bearing mounted on the azimuth axis of a gun turret is performed in order to understand the causes and mechanisms of friction in gun turrets. The bearing in question is a double row roller slewing bearing with two lip seals. Slewing bearing friction is caused by the torque due to applied load, viscous friction torque and seal friction torque.

Firstly, in order to measure friction torque of the slewing bearing, design and manufacturing of a friction measurement test setup is done. The setup consists of an electric motor, a torque sensor, a pinion gear, a bearing and mechanical parts for the assembly. In the detailed design stage, loads that are to be applied to the setup are calculated. According to the loads and requirements of test setup, proper motor and

torque sensor selections are undertaken. Since the tests are decided to be done at low speeds, the motor is equipped with a high ratio gearbox in order to have the capability to be used in high friction torque values.

Secondly, by using the friction measurement test setup, friction measurement tests are performed. Gun turret is expected to transfer the axial loading and tilting moment to the slewing bearing. So, the tests are performed in order to simulate these loadings. In total, 295 different tests are performed in order to observe friction torque of seals and bearing separately. Moreover, the effects of axial load, tilting moment and rotational speed on the friction torque are investigated.

Thirdly, friction torque analyses of the slewing bearing are done. In the analysis part, two different commercial codes are used: a finite element program called ANSYS and a multibody dynamic simulation program called ADAMS. In this part, the study is concentrated on friction torque caused by roller-raceway contact. Friction torque caused by roller-cage contacts and cage-ring contacts are neglected. In order to calculate the friction torque caused by roller-raceway contact, load distribution analyses are done in ANSYS. The load distribution analyses cover combined loading conditions. The roller loadings are used as input for ADAMS. In ADAMS, a simple model consisting of one roller and two raceways is generated. Between the roller and raceways, a friction force is defined. Moreover, a friction subroutine, which takes into account the lubrication regimes and determines friction force accordingly, is written in FORTRAN and implemented into ADAMS.

In the end, analysis and test results are compared and conclusions are drawn.

5.2. Conclusions

In order to examine the friction torque of the double row roller slewing bearing, several analytical and experimental studies have been performed. Effect of the upper seal, the lower seal and the bearing inner mechanism on the friction torque of the double row roller slewing bearing is separately investigated. Based on the tests and the analyses, the following results may be inferred.

- Causes of friction are separated as the bearing inner mechanism, the upper seal and the lower seal. According to the test results,
    - 34.5% of total friction is due to the bearing inner mechanism
    - 54.8% of total friction is due to the lower seal
    - 10.8% of total friction is due to the upper seal

    The test results clearly reveal that over 65% of the total friction torque of the slewing bearing is due to the seals. The total friction torque caused by the sealing elements is much higher than the torque caused by the bearing inner mechanism. Therefore, sealing selection of the slewing bearing is one of the most important steps to reduce friction torque. In addition, lower seal consists of a garter spring in order to increase the contact force of the seal. This is why the torque of the lower seal is much higher than the upper seal.
- Bearing inner friction torque is mainly caused by the roller raceway contact. So, the torque caused by roller-cage contact and cage-ring contact are neglected in the analyses. According to the test results, the bearing inner friction torque increases with the increase of any of the following: axial load, tilting moment and rotational speed.
- The analytical results show the same tendency with the test results. In the axial loading analysis, a maximum error of 6%; in the tilting moment analysis, a maximum error of 10% is recorded. So, the analytical method which uses one-roller model with appropriate contact parameters and friction force definition can be used to predict the friction torque of the slewing bearing under different loadings and rotational speeds. Moreover, similar experimental and analytical approaches can be applied for other types and sizes of bearings.
- The rollers used in the slewing bearing are of cylindrical roller bearings. In order to decrease friction torque of the bearing, tapered rollers may be used. In tapered roller bearings, rollers are tapered and raceways are manufactured as conical surfaces, which makes the motion of the raceways coaxial. Consequently, friction torque decreases by eliminating sliding between rollers and raceways.
- The proposed analytical model in this thesis requires use of two different analysis programs such as ADAMS and ANSYS. Both analyses are possible to

be performed by using one finite element analysis program. However, since implementing a user-written subroutine into ADAMS is easier for the author, in this thesis, friction identification analyses are performed by using ADAMS. In addition, for future works, complete modeling of the slewing bearing in a multibody dynamic simulation program will be much easier compared to finite element analysis programs.

In this thesis, the friction measurement tests are investigated and a method to calculate friction torque of a double row roller slewing bearing is presented. According to the results, the method proposed in this thesis seems as a reasonable way to make the initial guesses for the system designer to predict friction torque of the slewing bearing with an acceptable accuracy.

5.3. Future Work

In order to improve the work, there exist several aspects that need further investigation. Possible future work can be listed as:

i) Analyses and tests may be performed for high rotational speeds of the bearing in order to see a general trend for friction torque curve

ii) Full configuration of the bearing may be analyzed, by including friction torque due to cage-roller contacts and cage-ring contacts in the analytical model

iii) For given specific roller and lubrication type, a roller-on-disc experiment at different loading and speed conditions may be performed to have better accuracy of the analysis

iv) Finally, finite element analysis of the seals may be performed to have better understanding of friction characteristics of seals.

REFERENCES

[1] *Slewing Bearings* . Rothe Erde Gmbh, 2007.

[2] J. A. Williams and F. E. Kennedy, “Engineering Tribology,” *Journal of Tribology*, vol. 120, no. 3. p. 644, 1998.

[3] T. Harris, *Rolling Bearing Analysis*. John Wiley and Sons, Inc, 1991.

[4] *Modern Tribology Handbook Volume Two*. CRC Press, 2001.

[5] F. Guo, X. Jia, W. Longke, R. F. Salant, and Y. Wang, “The Effect of Wear on the Performance of a Rotary Lip Seal,” *J. Tribol.*, vol. 136, no. 4, p. 041703, 2014.

[6] E. Sincar, “Friction Identification and Compensation in Stabilized Platforms,” M.S. thesis, Middle East Technical University, 2013.

[7] J. I. Amasorrain, X. Sagartzazu, and J. Damián, “Load distribution in a four contact-point slewing bearing,” *Mech. Mach. Theory*, vol. 38, no. 6, pp. 479–496, 2003.

[8] S. Glodež, R. Potočnik, and J. Flašker, “Computational model for calculation of static capacity and lifetime of large slewing bearing’s raceway,” *Mech. Mach. Theory*, vol. 47, no. 1, pp. 16–30, 2012.

[9] R. Pandiyarajan, M. S. Starvin, and K. C. Ganesh, “Contact Stress Distribution of Large Diameter Ball Bearing Using Hertzian Elliptical Contact Theory,” *Procedia Eng.*, vol. 38, pp. 264–269, 2012.

[10] L. Kania, M. Krynke, and E. Mazanek, “A catalogue capacity of slewing bearings,” *Mech. Mach. Theory*, vol. 58, pp. 29–45, 2012.

[11] L. Kania, “Modelling of rollers in calculation of slewing bearing with the use of finite elements,” *Mech. Mach. Theory*, vol. 41, no. 11, pp. 1359–1376, 2006.

[12] J. Aguirrebeitia, M. Abasolo, R. Avilés, and I. Fernández De Bustos, “Theoretical calculation of general static load-carrying capacity for the design and selection of three row roller slewing bearings,” *Mech. Mach. Theory*, vol. 48, no. 1, pp. 52–61, 2012.

[13] P. Göncz, R. Potocnik, and S. Glodež, “Load capacity of a three-row roller slewing bearing raceway,” *Procedia Eng.*, vol. 10, pp. 1196–1201, 2011.

[14] R. Potočnik, P. Göncz, and S. Glodež, “Static capacity of a large double row slewing ball bearing with predefined irregular geometry,” *Mech. Mach. Theory*, vol. 64, pp. 67–79, 2013.

[15] P. Göncz, M. Drobne, and S. Glodež, “Computational model for determination of dynamic load capacity of large three-row roller slewing bearings,” *Eng. Fail. Anal.*, vol. 32, pp. 44–53, 2013.

[16] Y. Wang and Q. Yuan, “Contact Force Distribution and Static Load-carrying Capacity of Large Size Double Row Four-point Contact Ball Bearing,” *Def. Technol.*, vol. 9, no. 4, pp. 229–236, 2013.

[17] H. Allmaier, C. Priestner, C. Six, H. H. Priebsch, C. Forstner, and F. Novotny-Farkas, “Predicting friction reliably and accurately in journal bearings - A systematic validation of simulation results with experimental measurements,” *Tribol. Int.*, vol. 44, no. 10, pp. 1151–1160, 2011.

[18] H. Allmaier, C. Priestner, F. M. Reich, H. H. Priebsch, C. Forstner, and F. Novotny-Farkas, “Predicting friction reliably and accurately in journal bearings the importance of extensive oil-models,” *Tribol. Int.*, vol. 48, pp. 93–101, 2012.

[19] H. Allmaier, C. Priestner, F. M. Reich, H. H. Priebsch, and F. Novotny-Farkas, “Predicting friction reliably and accurately in journal bearings - Extending the EHD simulation model to TEHD,” *Tribol. Int.*, vol. 58, pp. 20–28, 2013.

[20] B. S. Ünlü and E. Atik, “Determination of friction coefficient in journal bearings,” *Mater. Des.*, vol. 28, no. 3, pp. 973–977, 2007.

[21] J. Shaona and C. Xiaoyang, “Friction moment analysis of space gyroscope bearing with ribbon cage under ultra-low oscillatory motion,” *Chinese J. Aeronaut.*, vol. 27, no. 5, pp. 1301–1311, 2014.

[22] T. Cousseau, B. Graça, A. Campos, and J. Seabra, “Friction torque in grease lubricated thrust ball bearings,” *Tribol. Int.*, vol. 44, no. 5, pp. 523–531, 2011.

[23] *SKF General Catalogue 6000 EN*. SKF, 2015.

[24] C. M. C. G. Fernandes, P. M. P. Amaro, R. C. Martins, and J. H. O. Seabra, “Torque loss in cylindrical roller thrust bearings lubricated with wind turbine gear oils at constant temperature,” *Tribol. Int.*, vol. 67, pp. 72–80, 2013.

[25] A. Joshi, B. Kachhia, H. Kikkari, M. Sridhar, and D. Nelias, “Running Torque of Slow Speed Two-Point and Four-Point Contact Bearings,” *Lubricants*, vol. 3, no. 2, pp. 181–196, 2015.

[26] S. Aihara, “A New Running Torque Formula for Tapered Roller Bearings Under Axial Load,” *J. Tribol*, vol. 109, no. July 1987, 2000.

[27] R. S. Zhou and M. R. Hoeprich, “Torque of Tapered Roller Bearings,” *J. Tribol.*, vol. 113, no. 3, p. 590, 1991.

[28] W. Qian, “Dynamic Simulation of Cylindrical Roller Bearings,” RWTH Aachen University, 2013.

[29] G. Marek, “On friction reduction in rubber lip seals for rotating shafts,” *Seal. Technol.*, vol. No. 40, pp. 8–11.

[30] S. Plath, S. Meyer, and V. M. Wollesen, “Friction torque of a rotary shaft lip type seal - A comparison between test results and finite element simulation,” *Mechanika*, vol. 4, no. 4, pp. 55–59, 2005.

[31] M. Silvestri, “Radial Lip Seals Efficiency Under Dynamic Operating Conditions,” in *International Conference on Tribology*, 2006, no. September.

[32] D. Frölich, B. Magyar, and B. Sauer, “A comprehensive model of wear, friction and contact temperature in radial shaft seals,” *Wear*, vol. 311, no. 1–2, pp. 71–80, 2014.

[33] C. Y. Lee, C. S. Lin, R. Q. Jian, and C. Y. Wen, “Simulation and experimentation on the contact width and pressure distribution of lip seals,” *Tribol. Int.*, vol. 39, no. 9, pp. 915–920, 2006.

[34] Y. Ke, X. Yao, H. Yang, and X. Liu, “Kinetic friction characterizations of the tubular rubber seals,” *Tribol. Int.*, vol. 72, pp. 35–41, 2014.

[35] “Brushless DC-Motors,” *Dunkermotoren GmbH*, 2014. [Online]. Available: http://www.dunkermotoren.com/data/downloads/catalogs/en/1508_Katalog_BG.pdf. [Accessed: 05-Nov-2015].

[36] “DR-2112 Torque Sensor Catalogue,” *Lorenz Messtechnik GmbH*, 2014. [Online]. Available: http://www.lorenz-messtechnik.de/pdfdatbl/m/080174ze_dr-2112.pdf. [Accessed: 05-Nov-2015].

[37] R. Budynas and K. Nisbett, *Shigley’s Mechanical Engineering Design*, vol. 8th Editio. 2006.

[38] B. J. Hamrock, S. R. Schmid, and B. O. Jacobson, *Fundamentals of Fluid Film Lubrication*, 2nd Edition. CRC Press, 2004.

[39] E. Claesson, “Modelling of roller bearings in ABAQUS", M.S. thesis, Chalmers University of Technology, 2014.

[40] L. Molnár, K. Váradi, G. Bódai, P. Zwierczyk, and L. Oroszváry, “Simplified modeling for needle roller bearings to analyze engineering structures by FEM,” *Period. Polytech. Mech. Eng.*, vol. 1, no. 2010, pp. 27–33, 2011.

[41] W. O. Winer and H. S. Cheng, *Film Thickness, Contact Stress and Surface Temperatures, Wear Control Handbook, 81-141*. New York: ASME, 1980.

[42] M. M. Khonsari and P. Kumar, “Lubrication regimes - line contacts,” *Encycl Tribol*, no. 2113–5, 2013.

[43] J. Takabi and M. M. Khonsari, “On the dynamic performance of roller bearings operating under low rotational speeds with consideration of surface roughness,” vol. 86, pp. 62–71, 2015.

[44] T. A. Stolarski, “Modern Tribology Handbook - Vol. 1-Principles of Tribology, Vol. 2- Materials, Coating, and Industrial Applications,..,” *Tribol. Int.*, vol. 36, no. 7, pp. 559–560, 2003.

[45] M. M. Khonsari and E. R. Booser, *Applied tribology-bearing design and lubrication*, 2nd Edition. Chichester, 2008.

[46] N. Patir and H. S. Cheng, “Application of average flow model to lubrication between rough sliding surfaces,” *ASME J. Tribol.*, no. 101, pp. 220–230, 1979.

[47] M. Masjedi and M. M. Khonsari, “An engineering approach for rapid evaluation of traction coefficient and wear in mixed EHL,” *Tribol. Int.*, vol. 92, pp. 184–190, 2015.

[48] T. Sakaguchi and K. Harada, “Dynamic Analysis of Cage Behavior in a Tapered Roller Bearing,” *ASME J. Tribol.*, vol. 128, no. July, pp. 604–611, 2006.

APPENDIX A

A. FRICTION FORCE SUBROUTINE

```
SUBROUTINE CFFSUB(ID, TIME, PAR, NPAR, LOCI, LOCJ, X, XDOT,
& NFORCE, AREA, DFLAG, IFLAG, FORCE)
C
C     === Type and dimension statements ==================
IMPLICIT NONE
INTEGER ID
DOUBLE PRECISION TIME
DOUBLE PRECISION PAR( * )
INTEGER NPAR
DOUBLE PRECISION LOCI(3)
DOUBLE PRECISION LOCJ(3)
DOUBLE PRECISION X(3)
DOUBLE PRECISION XDOT(3), KAR(2), AHMET(2)
DOUBLE PRECISION NFORCE
DOUBLE PRECISION AREA, AREA2
LOGICAL DFLAG
LOGICAL IFLAG
DOUBLE PRECISION FORCE(3)


C
C     Input parameters
C
C     ID      Identifier of calling CONTACT statement
```

```
C    TIME    Current time
C    PAR     Array containing passed parameters
C      PAR(1) - Marker1
C      PAR(2) - Marker2
C      PAR(3) - Reference Marker
C
C    NPAR    Number of passed parameters
C    LOCI    contact point location on I in I coordinates
C    LOCI    contact point location on J in J coordinates
C    X       sliding displacement since the beginning of contact
C      X(1) - translational deformation in x
C      X(2) - translational deformation in y
C      X(3) - rotational deformation about z
C    XDOT    slip velocity of contact point
C      XDOT(1) - slip velocity in x
C      XDOT(2) - slip velocity in y
C      XDOT(3) - relative angular velocity about z
C    NFORCE  contact normal force
C    AREA    area of contact
C
C    components returned to ADAMS
C
C    FORCE Array (dimension 3) of computed CNFORC
C      FORCE(1) - force in x direction
C      FORCE(2) - force in y direction
C      FORCE(3) - torque about z axis
C    Local variable and parameter definitions
C


DOUBLE PRECISION wl, Ea, Eb, poisson_a, poisson_b, ra, rb
DOUBLE PRECISION R_ro, R_ra, W, G, U, h_pe, h_ir, alpha, visc_0
DOUBLE PRECISION R, E_prime, wz, vx, vy, wz_i, wz_j, va, vb, ul
DOUBLE PRECISION vb_contact(2), B, h_c, h_min, Delta_lim, tao_lim
DOUBLE PRECISION ur, us, PI, visc, g_v, g_e, Delta, F1, F2
```

```
DOUBLE PRECISION h_prime, ss, F, p, z_1, sigma, L_a, p_h
DOUBLE PRECISION vick, V, y1, y2, y3, y4, y5, y6, y7, F_hd, F_bd
COMMON visc_0
INTEGER PAR1, PAR2
LOGICAL errflg, A
COMMON W, ra, alpha
C
C     ===Executable code ==================================
C
C
PI=4.D0*DATAN(1.D0)
Ea=2.03e11
Eb=2.015e11
poisson_a=0.24
poisson_b=0.28
ra=1000
rb=0.004
alpha=2e-8
visc_0=0.0288
R_ro=1.6e-7
R_ra=9e-8
B=0.0052265
wl=NFORCE/B
sigma=(R_ro**2+R_ra**2)**0.5
R=1/(1/ra+1/rb)
E_prime=2/((1-poisson_a**2)/Ea+(1-poisson_b**2)/Eb)
b=(8*R*NFORCE/PI/B/E_prime)**0.5
AREA2=2*B*b

C   PAR(1) = roller center marker
PAR1=PAR(1)
CALL SYSFNC('WZ', PAR1, 1, wz, ERRFLG)
CALL SYSFNC('VX', PAR1, 1, vx, ERRFLG)
CALL SYSFNC('VY', PAR1, 1, vy, ERRFLG)
```

```
C  Calculation of surface contact velocities for raceway
PAR2=PAR(2)
CALL SYSFNC('VX', PAR2, 1, va, ERRFLG)

vb=0.004*abs(wz)
ul=(abs(va)+abs(vb))/2/1000
us=abs(va-vb)

W=wl/E_prime/R
G=alpha*E_prime
U=visc_0*ul/E_prime/R
g_v=((G**2*W**3)/U)**0.5
g_e=(W**2/U)**0.5

y1=3*log10(g_v)-8*log10(g_e)
y2=3*log10(g_v)-4*log10(g_e)

CALL USRMES(.TRUE., "Ana Kod Tamamlandı", ID, "INFO")

c ----------------------RI Lubrication regime-----------------------

IF ( (log10(g_e) .LT. 0.2) .AND. (log10(g_v) .LT. 0.8) ) THEN
CALL USRMES(.TRUE.,"RI Lubrication Regime", ID,"INFO")
h_prime=4.9
visc=visc_0
h_min=h_prime*visc*R*ul/wl
ss=visc*us/h_min
F2=abs(ss*AREA2)

ENDIF
c----------------------- EI Lubrication regime -------------------

IF ( (log10(g_e) .GE. 0.2) .AND. (y2 .LE. 1.6) ) THEN
```

```
CALL USRMES(.TRUE., "EI Lubrication Regime", ID, "INFO")
h_prime=0.3*g_e**0.8
visc=visc_0
h_min=h_prime*visc*R*ul/wl
ss=visc*us/h_min
F2=abs(ss*AREA2)

ENDIF
c ----------------------- RV Lubrication regime ------------------

IF ( (log10(g_v) .GE. 0.8) .AND. (y1 .GE. 0.8) ) THEN
CALL USRMES(.TRUE.,"RV Lubrication Regime", ID,"INFO")
h_prime=1.66*g_v**(2/3)
b=(8*R*NFORCE/PI/B/E_prime)**0.5
p=NFORCE/(2*b*B)
z_1=alpha/(log(visc_0)+9.67)/(5.1*10**(-9))
visc=visc_0*exp((log(visc_0)+9.67)*(-1+(1+p*5.1*10**(-9))**z_1))
h_min=h_prime*visc*R*ul/wl
ss=visc*us/h_min
F2=abs(ss*AREA2)

ENDIF
c ------------------------- EV Lubrication Regime ------------------

IF ( (y1 .LT. 0.8) .AND. (y2 .GT. 1.6) ) THEN

CALL USRMES(.TRUE., "EV Lubrication Regime", ID, "INFO")
vick=7.25e9
V=vick/E_prime

y3=2.691*W**(-0.135)*U**(0.705)*G**(0.556)*R
y4=1+0.2*sigma**1.222*V**0.223*W**(-0.229)*U**(-0.748)*G**(-0.842)
```

```
h_min=1.652*W**(-
0.077)*U**(0.716)*G**(0.695)*R*(1+0.026*sigma**1.12*V**0.185*W**(-
0.312)*U**(-0.809)*G**(-0.977))
y5=0.005*W**(-0.408)*U**(-0.088)*G**(0.103)
y6=log(1+4470*sigma**6.015*V**1.168*W**(0.485)*U**(-3.741)*G**(-2.898))
L_a=y5*y6

Delta_lim=0.035
p=NFORCE/AREA2
p_h=p*(1-L_a/100)
tao_lim=Delta_lim*p_h

z_1=alpha/(log(visc_0)+9.67)/(5.1*10**(-9))
visc=visc_0*exp((log(visc_0)+9.67)*(-1+(1+p*5.1*10**(-9))**z_1))
b=(8*R*NFORCE/PI/B/E_prime)**0.5
y7=(L_a/100)*0.12+2*b*B*tao_lim/NFORCE*(1-exp(-visc*us/tao_lim/h_c))
F2=abs(NFORCE*y7)

ENDIF
C------------------------ Check for lubrication type -------
Delta=h_min/sigma;

IF (Delta .LT. 1) THEN
CALL USRMES(.TRUE., "Boundary Lubrication", ID, "INFO")
F1=(0.0008*NFORCE+0.0248)*vx+0.0288*NFORCE+1.0619
F_bd=F1/145/0.276
FORCE(1) = -abs(F_bd)

ENDIF

IF (Delta .GT. 5) THEN
        CALL USRMES(.TRUE., "Hydrodynamic Lubrication", ID, "INFO")
F_hd=F2
FORCE(1) = -abs(F_hd)
```

```
ENDIF
IF ((Delta .GT. 1) .AND. (Delta .LT. 5)) THEN
CALL USRMES(.TRUE., "Intermediate Lubrication", ID, "INFO")
FORCE(1) = -abs((F_bd-F_hd)/(1-5)**6*(Delta-5)**6+F_hd)

ENDIF
RETURN
END
```